Miniature gas sensing device based on near-infrared spectroscopy

Bassam Alfeeli

Thesis submitted to the Faculty of the Virginia Polytechnic Institute and State University in partial fulfillment of the requirements for the degree of

Master of Science
in
Electrical Engineering

APPROVED:

Anbo Wang, Chair
Gary Pickrell
Ahmed Safaai-Jazi

December 1, 2005
Blacksburg, Virginia

Keywords: Chemical sensing, optical fiber sensors, near-IR spectroscopy, molecular motion, the Beer-Lambert law, acetylene, hollow-core dielectric waveguides, fused silica capillary tubing

Miniature gas sensing device based on near-infrared spectroscopy

By
Bassam Alfeeli

Anbo Wang, Chairman
Electrical Engineering

Abstract

The identification and quantification of atoms, molecules, or ions concentrations in gaseous samples are in great demand for medical, environmental, industrial, law enforcement and national security applications. These applications require in situ, high-resolution, non-destructive, sensitive, miniature, inexpensive, rapid detection, remotely accessed, real time and continuously operating chemical sensing devices. The aim of this work is to design a miniature optical sensing device that is capable of detecting and measuring chemical species, compatible with being integrated into a large variety of monitoring systems, and durable enough to be used under extreme conditions.

The miniature optical sensor has been realized by employing technologies from the optical communication industry and spectroscopic methods and techniques. Fused silica capillary tubing along with standard communication optical fibers have been utilized to make miniature gas sensor based on near-infrared spectroscopy for acetylene gas detection.

In this work, the basic principles of infrared spectroscopy are reviewed. Also, the principle of operation, fabrication, testing, and analysis of the proposed sensor are discussed in details.

Acknowledgments

As a Virginia Tech student I would like to thank my committee members for their guidance and support during my research work at the Center for Photonics Technology (CPT).

I'm indebted to Professor Anbo Wang, Director of CPT, for giving me the opportunity to use the facilities and equipment available at CPT and for his encouragement, ideas and feedback throughout my research work and thesis. I'm grateful to Dr. Gary Pickrell, Associate Director of CPT, for many valuable discussions on photonics materials and experimentation. I also extend my appreciation to Professor Ahmed Safaai-Jazi for the many stimulating discussions on the theory of optical waveguides.

My sincere thanks go to all of my colleagues at CPT who help me through my experimental work especially, Fabin Shen, Xingwei Wang, Xiaopei Chen, and Yizheng Zhu.

Also as a staff member of the Kuwait Institute for Scientific Research (KISR), I would like to thank Mr. Hani Qasem, Manager of the Department of Advanced Systems (DAS) and Dr. Nader Al-Awadhi, Deputy Director General for Research Affairs, at KISR for giving me the opportunity to develop and enhance my scientific research skills by nominating me to get a Master's degree scholarship from KISR.

Finally, special thanks to both Mr. Eldon Andersen and Mr. Teodor Tichindelea, from Polymicro Technologies, LLC. They supplied my research with Polymicro's flexible fused silica capillary tubing.

Table of Contents

List of Figures

List of Tables

Chapter 1: Introduction

Sensors in general, and chemical sensors in specific, will be discussed in this chapter. Here the importance and the characteristics of chemical sensors will be examined. The classification of chemical sensors will also be illustrated.

1.1 Chemical Sensing

1.1.1 Definitions

The word sensor traces back to the Latin word ‘sentire’ which means ‘to perceive’. Technically, a sensor is “a device that responds to a physical or chemical stimulus such as heat, light, pressure, sound, magnetism or motion” [1]. A chemical sensor is a device that identifies a chemical species and quantifies the concentration of atoms, molecules, or ions in gases or liquids by producing a measurable signal [2].

1.1.2 The need for chemical sensors

The ability to detect and measure chemical species in situ is essential for any monitoring system [3]. Real time and continuously operating sensing devices are in great demand for medicine, process control [4], law enforcement, and national security applications. These applications require sensitive, non-destructive, rapid detection and quantification of the chemicals of interest [5]. Current sensing methods are expensive, time consuming, and limited in the sampling and analytical techniques. For example, according to the Sandia National laboratories, the Department of Energy (DOE) requires manual collection of nearly 40,000 groundwater samples per year in the Savannah River site. This can cost from $100 to $1,000 per sample for off-site analysis. Therefore, there is a need for inexpensive sensors that can be remotely accessed. Although commercial sensors are available for field measurements, only few have been adapted for long-term monitoring applications [6].

1.1.3 Characteristics of chemical sensors

The characteristics of sensors in general include stability, repeatability, linearity, hysteresis, saturation, response time, and span. However, chemical detection has two unique characteristics: selectivity and sensitivity. “Selectivity describes the degree to which a sensor responds to only the desired target species, with little or no interference from nontarget species. Sensitivity describes the minimal concentrations and concentration changes that can be successfully and repeatedly sensed by a device” [7]. Chemical sensors need to be both selective and sensitive to a specific species in a mixture of chemical species [7].

1.1.4 Classification of chemical sensors

Chemical sensors can be classified into two major groups, chemically reactive devices and physically reactive devices [7]. Figure 1-1 shows the two major groups of chemical sensors and some of their subclasses.

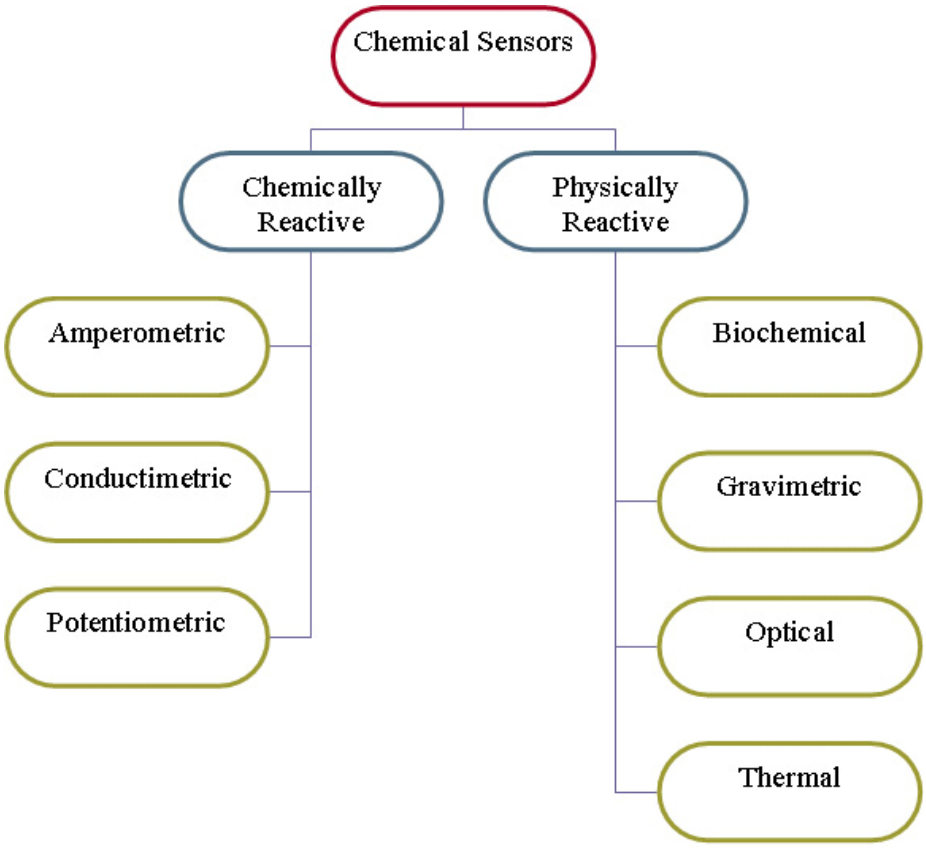

Figure 1-1 Classification of chemical sensors

1.1.4.1 Chemically reactive (electrochemical) sensors

This group is also called electrochemical sensors. In this group the sensing element reacts chemically with the chemical species to produce a measurable signal. These sensors inherently suffer stability problems such as incomplete reversibility, depletion of the sensing element, or interference from other species.

This group is further sub-grouped by the electrical characteristics of the sensing element. Sensors that measure change in electrical or electronic current are called amperometric. Sensors that measure change in resistance or impedance are called conductometric. Sensors that measure change in electrical potential or voltage are called potentiometric [7].

1.1.4.1.1 Amperometric

Amperometry is an electro-analytical technique that consists of two electrodes immersed in a suitable electrolyte [8]. It's used to sense liquid and gas species. The process of oxidization or reduction governed by Faraday's Law produces or consumes electrons at the electrodes. The sensor is controlled by a potentiostatic circuit which produces a current or signal when the sensing element exposed to the species contains the electroactive analyte. For ppm level reactants, the sensor produces current at the micro or pico ampere level. Its response time ranges from milliseconds to several minutes. The amperometric gas sensor is used for detection of toxic gases such as CO, NO, NO_2, H_2S, SO_2, and O_2 [2]. However, this class of sensors is a more cumbersome choice for sensing, mainly because it is a high-impedance current source. Hence, they need to be grounded and shielded. Further, since temperature affects the rate of chemical reactions, they are sensitive to temperature variations [8].

1.1.4.1.2 Conductometric

Conductometric sensors work based on the principle of conductivity change in solids or electrolytes by chemical reaction with target species. The conductance is measured at both terminals of the sensing element in a current at applied voltage or a bridge arrangement. In solid state conductometric sensors, the selective layer can be, but not limited to, metal oxide semiconductor (MOS), solid electrolyte, or conducting polymer

(CP). The overall resistance of the device can be chemically modulated by the selective layer itself. This can be done through modulation of the bulk conductivity or surface conductivity [9]. Solid state sensors have advantages such small size, low cost, low power consumption, and simplicity in operation. However, they lack stability, reproducibility, selectivity and sensitivity [10].

1.1.4.1.2.1 Chemical field effect transistor (ChemFET)

Chemical field effect transistor has a gas selective coating between the transistor gate and the analyte. This chemical element modifies the source-drain conduction in relationship with selected chemical species. The sensor's conductance is measured by a differential amplifier. ChemFET can detect H_2 in air, O_2 in blood, NH_3, CO_2, and explosive gases [7]. This sensor is attractive since it's rugged, batch-fabricated and disposable. In addition to the general disadvantages of solid state sensors, ChemFET is not biocompatible and suffers drift and degradation with time. In the present time, FET-based sensors are not suited for log-term, in-line chemical analysis [10].

1.1.4.1.2.2 Organic conducting polymers (CPs)

Most polymeric materials are not good conductors. However, there are some conducting polymeric materials. Conductivity may be an intrinsic property of the material or it may result from adding conductive filler to the polymeric matrix. Similar to semiconductors, polymers may also be doped and the conductivity depends on the doping level. However, electronic conduction in polymers cannot be explained by the band theory. This is because the atoms in conducting polymers are covalently bonded forming a chain that experiences weak intermolecular interaction. Electrons are required to move along the chain and from one chain to another for conduction to occur. The CP chemical sensor responds in two different ways depending on the gas species. First, Nucleophilic gases causes an increase in the CP's resistance and electrophilic gases cause a decrease in the CP's resistance. This process is reversible at room temperature. Second, some chemical species have a solvent type action on the polymer, making it swell. Changes in the CP's dimension change the conductivity of the material [1]. The CP sensor response time ranges from 2 to 15 seconds. The sensor is reusable since it returns to its normal state

when it's no longer in contact with the chemical species. Also, it consumes less power than metal oxide sensors. On the other hand, the sensor is not corrosive resistant, must be agent specific at certain concentrations, and is insensitive to gases like O_2, Cl_2, H_2, and NO [7].

1.1.4.1.2.3 Thin-Film Metal-Oxide Semiconductor (MOS)

Metal-Oxide Semiconductor sensors work under the principle that metal oxides change their electrical properties in the presence of reducible gases. For example oxygen is adsorbed on the surface of SnO_2 at certain high temperatures in air, and surface potential is formed that restrains the flow of electrons. As the surface is exposed to reducible gases, the surface potential decreases and the conductivity increases. These sensors are simple and rugged devices but require electronic circuit to operate [7]. They also require elevated temperatures (200-500 °C) for their operation, and have slow response time which is limited by the chemical reaction rate [2].

1.1.4.1.3 Potentiometric

The process of charge separation produces potential difference. The partitioning of the electrically neutral molecules to ions and electrons at the sensing element yields potential change [9]. The main component of this technique is an ion conducting membrane (ion selective electrode) which separates the target species from the inside of the electrode. The inside of the electrode is an electrolyte solution containing the ion of interest at a constant level, see figure 1-2. The charge separation at the interface between the membrane and the target species results in measurable potential against the fixed potential of the reference electrode. Thus, the measurable potential under zero current conditions can be related to the ion level of the target species [11]. This kind of sensor is simple in principle of operation and construction. It's also used to sense gaseous or liquid samples. The sensor detects the target gas by measuring the local ion-activity variation due to gas molecules hydrolysis. For a CO_2 sensor, a hydrogen ion selective electrode or bicarbonate selective electrode is used to monitor the changes in the ion activities. The dissociation of one mole of CO_2 yields one mole of hydrogen or bicarbonate ion. The response time of the sensor is in the range of 10 to 20 seconds [9]. This class of sensors

responds in a logarithmic fashion to the target species. Unless the ionic strength is known, the concentration cannot be calculated. They also suffer from incomplete selectivity due to ion interference from other species and potential drift due to variation in liquid junction potential and temperature [8].

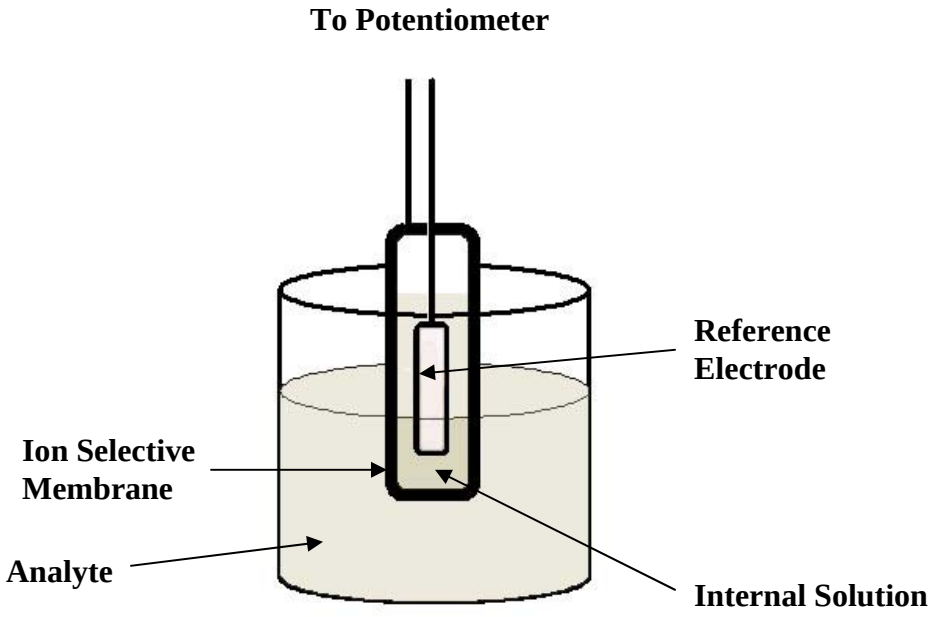

Figure 1-2 Potentiometric Sensor

1.1.4.2 Physically reactive sensors

In this group the sensing element isolates and employs a physical reaction to indicate the existence of a chemical species. These sensors have less stability problems but have slower reaction time and require additional instrumentation [7].

1.1.4.2.1 Thermal

This class of sensors "uses the heat generated by a specific reaction as the source of analytical information" [9]. This technique is known as microcalorimetry. By coating a temperature probe with a chemically selective layer, the probe measures the release of heat during the reaction between the sample and the coating. The measurement can be either as the change in temperature or as the heat flux through the sensing element. They are stable, inexpensive, sensitive, and small. They cover a temperature range from -80 to 350 °C and have a negative or positive temperature coefficient. They must be a

thermodynamically open system, thermally insulated, and protected from chemical poisoning [9].

1.1.4.2.2 Gravimetric

Gravimetric, also known as mass, piezoelectric, or acoustic wave, sensors work based on the relationship between the resonant frequency of an oscillating piezoelectric crystal and the mass deposited on the crystal surface. When the acoustic waves are excited in the piezoelectric crystal by an electronic oscillator circuit, the resonant frequency of the crystal can be measured [11]. The bounded acoustic waves must satisfy certain boundary conditions. “The most important boundary condition is that all stresses normal to the surfaces must be zero” [8]. The addition or subtraction of foreign material on the crystal surface alters both the effective thickness and the surface boundary condition which results in change in the resonant frequencies of the device. This change can be measured by placing the resonator in the feedback loop of an oscillator circuit which will undergo a frequency shift in response to perturbation [8]. Frequency shift measurement is one of the most accurate types of physical measurement. This class of sensors has advantages such as light weight, low power consumption, low cost, and design flexibility. Unlike electrochemical sensors, the measurement is conducted by a single physical probe. However, if the interaction of the chemical species with the crystal surface is a replacement of one species with another of a similar mass, the net change of mass may be very small. They are very susceptible to external pressure, humidity, and temperature. [9]. They have poor reversibility and slow response time.

Surface acoustic wave (SAW) devices have better detection sensitivity since they can be operated at much higher frequencies. A SAW sensor can achieve a mass change resolution of 3 femto-grams [8]. This translates to a detection limit of better than 0.05 ppm [11]. It has been used to detect inorganic gases such as NO_2, H_2, H_2S, and SO_2 and organic gases such CH_4, C_6H_6, and C_2H_5OH [2].

1.1.4.2.3 Biochemical

Biochemical sensors are a special class of chemical sensors. They are analytical devices that combine biologically active materials with several physical sensing measurements

such as weight, electrical charge, potential, current, temperature or optical activity [10]. The biologically active material can be organisms, tissues, cells, organelles, membranes, enzymes, receptors, antibodies, and nucleic acids. The sensing element is a bioreactor on top of a conventional sensor. The response is determined by the diffusion of the analyte, reaction product, and interfering species. One of the biggest challenges in the biosensor area is immobilization of the analytes on the physical sensing element. "The biologically active material must be enclosed within and kept from leaking out the sensing element over the lifetime of the biosensor" [7]. Immobilization should not denature the biologically active material and must also allow contact to the analyte solution, and allow any product to diffuse out [7]. Some of the unique advantages of this kind of sensors are biocompatibility, sterilizability and high accuracy. Concentrations below 0.5 ppm can be detected. Nevertheless, these sensors tend to have long response time, short life time, poor reversibility and stability, and specific operating temperature. These sensors have been used to detect O_2, CO_2, NH_3, CO, NO_2, and H_2S [10].

1.1.4.2.4 Optical

The interaction of electromagnetic radiation with matter results in altering some properties of the radiation. Optical sensors use this interaction to provide information about the sample under study [9]. Optical sensing devices can be categorized into five categories based on the way they modulate light. Figure 1-3 shows the five optical modulation schemes.

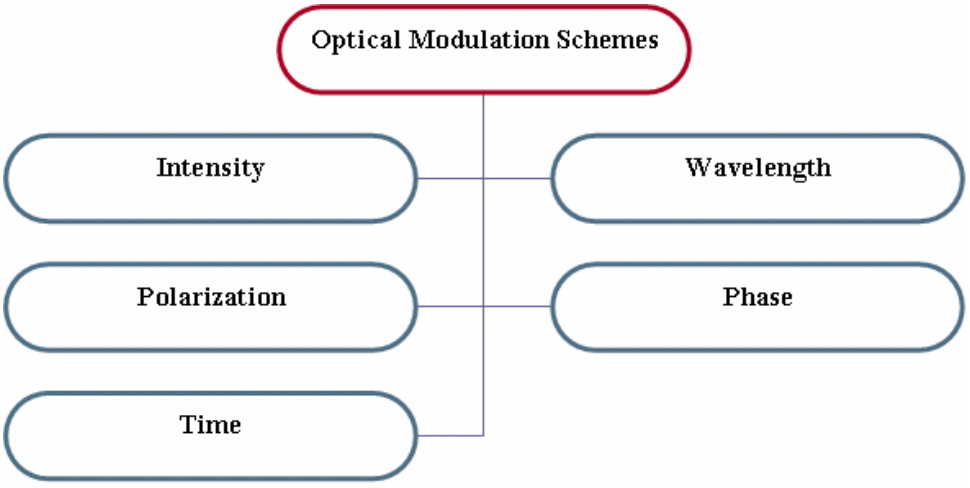

Figure 1-3 Optical Modulation Schemes

The detection technique and the source requirements are prescribed by the modulation scheme. Table 1-1 summarizes the different schemes, their detection methods and limitations. Further, different sensors have different measurement techniques and use different physical parameters that cause light modulation. The measurement techniques, the light modulation type, and the physical modulation parameters are tabulated in table 1-2 [12].

Optical sensors have many advantages over other chemical sensors. Optical signals are immune to electromagnetic interference, temperature variations, generally do not disturb the process measured, and interact with matter on the atomic and molecular levels. Some optical techniques can achieve a detection limit of 0.027 ppm or even detecting a single molecule. Thus, they provide information with high sensitivity and selectivity. Further, the ready availability and continuous development of optical components and instrumentations from the optical communication industry give an economic advantage to optical sensors. Furthermore, the use of waveguides adds more advantages to optical sensing. Optical waveguides can be produced from different materials such as glass, plastic and single crystals. They are inexpensive (single crystal fibers are an exception), robust, flexible, chemically inert, and biocompatible. They also have small physical dimensions, and can be sterilized. Waveguides, such as optical fibers, capillary tubes and planer waveguides, can deliver light to and from the active sensing element over large distances at different locations via multiplexing. This enables real-time, on-line, and multipoint monitoring of large structures and sensing in remote areas that are hazardous, hostile, or difficult to access. Optical sensors have been used to detect many gases such as O_2, O_3, N_2, CO, CO_2, H_2S, HCl, CH_4, C_2H_2, N_2O, and NH_3, just to mention a few [2], [8], [9], [12], [13], [14].

Table 1-1 Optical Modulation Schemes and Detection Techniques
[12]

Type of Information	*Physical Mechanism*	*Detection Circuitry*	*Main Limitations*
Intensity (*I*)	Modulation of number of photons transmitted after absorption or emitted by luminescence, scattering, or refractive index change	Analog detection	Normalization for source intensity variations and variable line and connector losses
Wavelength (λ)	Spectral-dependent variations of absorption and fluorescence	Amplitude comparison at two (or several) fixed wavelengths, or continuous wavelength scan	Wavelength-dependant line losses; suitable scanned-wavelength sources or spectrometers
Phase (ϕ)	Interference between separate paths in Mach-Zehnder, Michelson, Fabry-Perot interferometers	Fringe counting, or fractional phase-shift detection	Stability and measurement of small phase shifts; coherent source and detection methods
Polarization (*p*)	Change in rotation of polarization	Polarization analyzer and amplitude comparison	Random polarization changes in line (induced birefringence in fibers and components)
Time resolved (*t* time domain, ω frequency domain)	Transient behavior (lifetime) of luminescence or absorption	Analysis of time-decay amplitude signal	Model time dispersion in fibers; low intensity signal

Table 1-2 Principal Chemical Measurement Techniques and Types of Light Modulation [12]

Chemical Measurement Technique	*Light Modulation*	*Parameter Modulation*
Absorption, scattering, reflectance	***I***	
Colorimetry, spectrometry (absorption, Raman, SERS), fluorimetry, luminescence	***I***, λ	
Refractometry	***I***	*n*
Interferometry	*I*, ϕ	*n*, *L*
Special Interferometry	*I*, ϕ, λ	*n*, *L*
Polarimetry	*I*, ***p***	
Ellipsometry	*I*, ***p***	*L*
Photokinetics	***I***, ***t***	
Reflectometry	***I***, *t*	*L*
Combined refractometry and reflectometry	***I***, *t*	*n*
Evanescent spectroscopy, SPR	***I***, λ	*n*
Lifetime-based fluorimetry	***I***, λ, ***t***	
Flight-time fluorimetry	***I***, λ, ***t***	*n*
Polarized lifetime-based fluorescence	***I***, λ, ***p***, ***t***	
Photoacoustic	***I***, ν	*P*

Notes: Abbreviations are as follows: SERS = surface-enhanced Raman spectroscopy. SPR = surface plasmon resonance.
Light modulation: *I* = intensity, λ = wavelength, ϕ = phase, *p* = polarization, ν = optical frequency, and *t* = time. (The main type of modulation is indicated in bold type.)
Physical parameter modulation: *L* = path length, *n* = refractive index, *P* = pressure.

Optical sensors also have several limitations. In general, this class of sensors provides information about concentration (number of molecules per unit volume in the sample) as the main effect of interaction with light. Only secondary effects such as line broadening, fluorescence decay time variation, absorption, and/or emission peak shift, can provide some information about the molecules interaction among themselves and with their

environment. Yet, there is no general relationship between the molecule activity coefficient in a given environment and these secondary effects [9]. Therefore, this remains a disadvantage of optical sensors. Moreover, optical signals can be influenced by stray ambient light, absorption due to noncolloidal particles dispersed in the analyzed medium, and unwanted background fluorescence. Photo-degradation, self-absorption, and inner filter effects inside the sample can also affect the optical signal [12].

1.1.4.2.4.1 Classification of optical sensing elements

The optical sensing elements can be classified into intrinsic and extrinsic groups. In intrinsic element sensors, the light interacts with matter within the optical component. In waveguides, the light interacts with the sample while being guided in the fiber. If the waveguide only delivers light to and collects it from the sample then it's called an extrinsic sensor. Thus, in extrinsic element sensors, the light interacts with matter outside the optical component [12].

1.1.4.2.4.1.1 Intrinsic element sensors

1.1.4.2.4.1.1.1 Refractometric sensors

Refractive index measurements can be used to detect chemical species. The sensing element measures, at the waveguide-to-analyte interface, the critical angle at total internal reflection or the change in the angle at non-critical reflection. The refractive index can then be determined based on the Snell's law and these measured parameters. Sensing elements such as unclad fibers bent in U-shape, or in spiral form, twisted fibers, and tapered fibers have been used in refractometric sensors [12].

1.1.4.2.4.1.1.2 Evanescent-wave sensors

The continuous evanescent field in the core-cladding interface of the waveguide can be used to measure changes in the optical properties of the area within this field. The cladding can be a chemically sensitive layer or the sample itself. The evanescent field depth and the optical path length determine the magnitude of the interaction between the light and matter. The optical path length depends on the wavelength, geometry, and

refractive indices of the material used in the sensor [9]. The sensor reported in [15] is one of many configurations that have been realized recently.

1.1.4.2.4.1.1.3 Hollow-core sensors

Hollow waveguides with their inner surface coated with a chemically sensitive layer can be used as sensors. The cavity confines and guides both the light and sample. One possible configuration of this type of sensors is reported in [16]. Liquid core fibers can also be used as a detection device. However, for the light to be guided, the liquid has to have a refractive index greater than the clad. Liquid solvents such as CS_2 (n = 1.628) or toluene (n = 1.494) have been used as a liquid core [12].

1.1.4.2.4.1.2 Extrinsic element sensors

1.1.4.2.4.1.2.1 Sensing cells sensors

A sensing cell consists of a light source and receiver facing each other across a gap which contains the sample. The light passes through the cell in a single or multiple pass configuration. The use of optical fibers allows short optical path length and small volume sensing cells [12].

1.1.4.2.4.1.2.2 Reagent-based sensors

There are several ways to place active chemical or biochemical layers on the sensing element. The reagents are deposited between supporting polymeric matrices and membrane materials to immobilize them. Glucose, pH, and immunoassay sensors are some examples of this class of sensors [8].

1.2 Thesis objectives, scope and overview

The objectives of this thesis are to explore chemical sensing based on optical techniques and investigate the possibility of making a miniature chemical sensor from fused silica capillary tubing. This research focuses on acetylene gas sensing based on near-infrared spectroscopy. The thesis is organized by the following chapters:

Chapter 1: Chemical sensing. This chapter defines sensors in general and chemical sensors in specific, examines the importance and the characteristics of chemical sensors, and classifies the different types of chemical sensors.

Chapter 2: Sensor design. This chapter covers the sensor design goals and requirements. It also gives an overview of IR gas sensing in general, explains the principle of operation of the sensor, and explores near-IR spectroscopy.

Chapter 3: The acetylene molecule. This chapter identifies the molecule's structure and its chemical and physical properties.

Chapter 4: Experimental results. This chapter gives a detailed description of the experimentation procedures and results that determined the dimensions of the miniature gas sensor.

Chapter 5: Analysis. This chapter discusses the analysis of the experimental results.

Chapter 6: Conclusions and future work. This chapter concludes the work presented in this thesis and suggests areas of further research and development.

Chapter 2: Sensor design

The design goals and requirements will be identified in this chapter. This will set up the stage to develop a sensor that meets the thesis objectives.

2.1 Design goals

The design goals are to design a miniature device in which it has the capability of detecting and measuring chemical species, the compatibility of being integrated into a large variety of monitoring systems, and the durability to be used under a wide rage of environmental conditions.

2.2 Design requirements and approach

To meet the design goals, the sensor design should satisfy the following requirements. The sensor should be:

1. Robust
2. Flexible
3. Inexpensive
4. In the millimeter size range
5. Remotely accessed
6. Chemically inert
7. Biocompatible
8. Immune to the electromagnetic interference
9. Unaffected by temperature variations
10. Non-destructive
11. Sensitive
12. Selective
13. Fast with respect to response time

Assuming adequate selection of components and proper integration and packaging, the optical communication industry provides the technologies needed to satisfy the first eight requirements. These technologies utilize components and instruments that operate in the

infrared (IR) region of the electromagnetic spectrum. The rest of the design requirements can easily be satisfied by spectroscopic methods and techniques. Sections 2.3 and 2.4 provide some background on IR sensing and spectroscopy.

In order to choose the most appropriate design the sample and the sampling method should be considered. The quality of the measurement is strongly dependent on the method of sample preparation and the interface between the sample and the sensor. It must be appreciated that the sample's physical state and how the sample is treated influences the sensor's response [17].

2.2.1 Sample characteristics

Samples in the gaseous state are easy to handle. The main issues are pressure, temperature, and the relative concentrations of other species in the sample. One should also pay attention to the sample's physical and chemical properties. The optical properties of the sample determine the depth of penetration of the light beam and affect the wavelength of the light and path length. Care should be taken due to the possible corrosive or explosive tendencies of the sample. The chemical reactivity determines the materials that can be used in the sensor. In this design a clear sample in the gaseous state is being assumed. Also, it's assumed that the materials used in the sensors are inert to the sample [17].

2.2.2 Sample presentation geometry

There are many sample presentation methods. The main sample presentation methods are transmission and reflection. Clear samples are typically measured by the transmission method. Gaseous samples need to be contained in a gas cell. A traditional gas cell is a glass or stainless steel tube with transmission widows at both ends. The cells are usually evacuated with a vacuum pump and the filled with sample to the desired pressure. A gas cell will be implemented in this design. The gas cell should be clean in order for the light beam to travel through without any obstruction and should only contain the sample under study [17].

2.2.3 Data acquisition and signal processing

Data acquisition depends on both the sample and the sensor's operation. To monitor the presence of gaseous samples, one needs a real-time, very fast, high resolution, and high signal-to-noise ratio system. The implementation of spectroscopy in the design demands a system capable of transmitting IR radiation to the gas cell, and then detecting the signal with a high dynamic range detector. The system should also have the ability to resolve spectral information. Since fiber optics technology is being considered in the design, a component testing system (CTS) would be a good choice for data acquisition and signal processing. The system has a radiation source and a detector that works in the desired spectral range. A straightforward transmission measurement should provide sufficient data quality to meet the design requirements. Also, the basic, unprocessed spectral data should be adequate for monitoring and detection purposes [17].

2.3 Infrared gas sensing

IR gas sensing devices are in general classified as extrinsic, absorption based, and intensity modulated optical sensors. The use of IR technology in gas sensing is considered one of the most important technologies in industrial, environmental, and safety monitoring [18]. It has been used to provide high-resolution, non-destructive, sensitive, and fast detection and quantification of important chemical species [5].

All transparent materials, including perfectly transparent materials, alter the electromagnetic radiation as it passes through them. The properties of the transmitting medium determines the amount of change in the radiation energy [11]. As light passes through a gas cell, fragments of the light energy will be absorbed by the gas molecules resulting in distinctive absorption bands in the absorption spectrum which enables recognition of the chemical species. Every chemical species has its own unique absorption spectrum. The presentation of the absorbed radiation at each wavelength, as a function of wavelength, is called absorption spectrum. For a device to produce such a spectrum, it has to consist of a radiation source, a defined optical path (sample cell), and a detector [19].

The IR region of the electromagnetic spectrum is divided into three spectral regions. The far-IR region extends between 1mm to 50 μm. The mid-IR region extends between 50 μm to 2.5 μm. The near-IR region extends between 2.5 μm to 780 nm. The different regions of the IR spectrum cause different molecular perturbations when they interact with matter [20].

2.3.1 Far-IR

The difficulties of generating and detecting far-IR made it the least studied part of the electromagnetic spectrum. Far-IR is used to study resonances in crystals such as cyclotron and antiferromagnetic resonances, energy band gap in superconductors and plasma [21]. It excites the stretching vibrations of heavy-atoms molecules, the crystal lattice vibrations, and the central atom-ligand vibrations of inorganic compounds and metalorganic complexes. The spectrum is limited by the low energy generated from the heat sources and the materials of the optical components [22]. An important disadvantage of far-IR is it can be absorbed by almost everything. This results in loss of the transmitted radiation energy.

2.3.2 Mid-IR

By far mid-IR is the most commonly used region in IR spectroscopy. It provides rich and specific chemical information on individual chemical species [23]. The spectra can be obtained from small samples but requires sample preparation. Mid-IR excites the fundamental vibration modes of molecules. It has higher sensitivity compared to near-IR. The absorption band intensity increases by a factor of 10-100 by going from near-IR to mid-IR. Nevertheless, mid-IR is limited by the materials used to make the optical components [22].

2.3.3 Near-IR

Near-IR has only recently become popular. It has been used in chemistry, the oil industry, and biological and medical analysis [22]. Near-IR excites the overtone and combination of the fundamental vibrations of molecules. The optical components for this region can be easily obtained from the fiber optic industry [23]. However, only a small number of

chemical species have absorption bands in this region [20]. The near-IR region will be considered in the design.

2.4 Near IR spectroscopy

Since near-IR is being considered in the sensor's design, the following section provides an overview of near-IR spectroscopy.

Many disciplines utilize IR spectroscopy in solving problems related to their fields. Physicists use it to study the energy levels in semiconductors, to determine inter-atomic distances in molecules, and to measure the temperature of flames. Chemists use it to determine isomers, to characterize wax, resin, and polymers, to fingerprint organic compounds, and follow the progress of a reaction. Biologists use it to study transport of materials in living tissue, and to study the structures of cells and antibiotics [24].

A complete presentation of the theory of IR spectroscopy requires an extensive background in mathematics, quantum mechanics, chemistry, and molecular physics to understand and appreciate the concepts involved. Therefore, the author chooses to limit the scope of the theoretical coverage to gas samples in the near-IR region that consists of polyatomic linear molecules with permanent dipole moments.

2.4.1 Definition of spectroscopy

Spectroscopy includes the methods and techniques that deal with interactions of matter with electromagnetic radiation in the form of absorption, emission, and scattering of radiation energy [25]. Near-IR spectroscopy is the spectroscopic method and technique that utilizes the near-IR region.

2.4.2 Molecular structure, motion, and energy

A simple picture of a molecule cannot be drawn due to the complicated quantum mechanical description of molecular structure. Yet, a model based on classical mechanics should be enough to understand the basic spectroscopic relationships. Molecules are composed of two or more atoms held together through interaction of the electrons in the outermost orbital shells [22]. Molecules can move in the following types of motion: translation of the whole molecule, which can be regarded as translation of the center of

mass, rotation of the molecule as a framework around its center of mass, and vibrations of individual atoms within the framework [26]. The translational motion is not considered here since it is not of direct concern in IR spectroscopy. The other two types of motions are quantized and have frequencies that coincide with the frequencies of the IR region. The vibration of atoms can be excited by absorption of energy from electromagnetic radiation. When the energy absorbed is not enough for vibrational excitation, the rotation of molecules gets induced [22].

2.4.2.1 Molecular vibration

The classical concept of molecular vibration is thought of as point masses, which represent atoms, linked together by weightless elastic springs, which represent the bonds between the atoms [22]. For polyatomic molecules, there are various vibrational possibilities which can be traced back to a definite number of periodic vibrations called normal vibrations. The molecular vibration results from the superposition of these normal vibrations. In normal vibrations, atoms undergo near-harmonic vibration of identical frequency in identical or opposite phase along the straight line passing through the equilibrium position. In linear molecules, the displacement of the atoms occurs in the direction of the valence bond which increases and decreases the bond distances periodically. Vibrations such as these are called stretching vibrations [27].

For simplicity, it is necessary to assume that the atoms are harmonic oscillators with restoring forces that obey Hook's law. Further, each atom can move in three spatial directions. Thus, a molecule with N atoms has $3N$ degrees of freedom available. Three of these degrees of freedom are used to represent the center of mass of the molecule and another three to represent the rotational position of its axis. Therefore, the actual number of vibrational degrees of freedom is $3N-6$. In linear molecules, the rotation around the molecular axis is not associated with any movement of the center of mass of the atoms. This makes them have only two rotational degrees of freedom. Hence, this type of molecules has an extra vibrational degree of freedom, $3N-5$.

For any given configuration of atoms, it is possible to have a set of $3N-5$ generalized coordinates Q_i such that the potential energy V and the kinetic energy T may be written as

$$V = \frac{1}{2}\sum_i f_i Q_i^2 \tag{1}$$

$$T = \frac{1}{2}\sum_i Q_i^2 \tag{2}$$

where f_i 's are the constant in Hook's law and they are the roots of a determinantal equation of order $3N-5$ known as secular equation. There are also no cross-products terms of the coordinates $Q_i Q_j$. The set of Q_i are known as normal coordinates. When, in turn, each of Q_i 's is alone allowed to vary, the molecule undertakes normal vibrations. During vibration, kinetic and potential energy are constantly interconverted just like in a pendulum. The sum of the two forms of energy remains constant thus,

$$T + V = 0 \tag{3}$$

Since describing molecular motion with classical mechanics is not sufficient, quantum mechanical treatment is needed. The Schrödinger equation assigned to the system is given by

$$\sum_i \frac{\partial^2 \psi}{\partial Q_i^2} + \frac{8\pi^2}{h^2}\left(E - \frac{1}{2}\sum_i f_i Q_i^2\right)\psi = 0 \tag{4}$$

Equation 4 can be separated into $3N-5$ one-dimensional equations since there are no cross-products of the coordinates. For each of these equations, the eigenvalues are as given by that of a simple one-dimensional harmonic oscillator. Thus,

$$E = \sum_i \left(n_i + \frac{1}{2}\right) h\nu_i \tag{5}$$

where the n_i 's are the vibrational quantum numbers and ν_i 's are the frequencies of the normal vibrations. The quantum mechanical selection rule governing the harmonic vibrational transitions is $\Delta n = \pm 1$; all other transitions are forbidden. The normal vibrations frequencies ν_i 's are given by

$$\nu_i = \frac{\sqrt{f_i}}{2\pi} \tag{6}$$

The calculation of the values of f_i 's in any given case may be very complicated but could be simplified by using the theory of symmetry groups [21].

A triatomic linear molecule can have four vibrations, see figure 2-1.

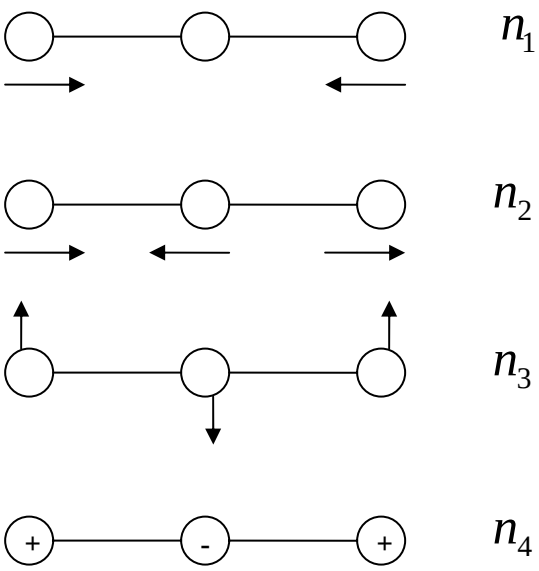

Figure 2-1 Vibrational modes of a triatomic linear molecule

In the first mode of vibration, the symmetrical movement of both outer atoms away from or towards the central atom valence direction causes no movement in the molecule. Since no dipole moment change is associated with this vibration, it cannot be excited by IR radiation and thus is called infrared-inactive vibration. In the second mode of vibration, the outer atoms move antisymmetrically with respect to the central atom. This movement

induces a dipole moment which makes it an infrared-active vibration. In the third mode of vibration, atoms move perpendicular to the valence direction where both outer atoms move in the opposite direction of the central atom. This results in 180º change of the valence angle in equilibrium. Dipole moment is also induced for this vibration making it an infrared-active vibration. The fourth mode of vibration is similar to the third mode except that the direction of motion of the atoms in n_4 is turned 90º out of the figure plane. Although n_3 and n_4 vibrations must assume the same value, they are considered different normal modes of vibration since they are described by different spatial coordinates. When such vibrations occur at the same frequency, they are called degenerate vibrations [22].

The forces between atoms cannot be described accurately by simple force constant. In fact actual molecules do not conform to the simple harmonic model [28]. Therefore, molecules in reality are anharmonic oscillators. The effect of anharmonicity can be seen either as the crowding of the higher energy vibrational levels or as the permitted transitions of more than one vibrational quantum. This is in contrast to the equally spaced vibrational levels and the forbidden transition of more than one vibrational quantum in the harmonic model. Hence, actual molecules at room temperature are not limited by the transition from 0 to 1, they also have transitions from 0 to 2, 3, etc. at approximately twice, three times, etc the frequency of the longest wave band. The transition from 0 to 1 is called fundamental and transitions from 0 to 2, 0 to 3, etc. are called overtones [25]. To account for the anharmonicity effect, an extra term is added to equation 5

$$E = \sum_i \left(n_i + \frac{1}{2} \right) h\nu_i - \left(n_i + \frac{1}{2} \right)^2 h\nu_i x_i \qquad (7)$$

where x_i is the anharmonicity constant which gives a measure of the change in bond strength with the change in the interatomic distance [29].

2.4.2.2 Molecular rotation

The rotation of linear polyatomic molecules is exactly the same as that for diatomic molecules. Thus, in this section the rotation of diatomic molecules will be considered. In general any diatomic molecule has three moments of inertia I_a, I_b, and I_c about three mutually perpendicular axes, see figure 2-2. For linear molecules, $I_a = 0$ and $I_b = I_c$, where I_b is defined as

$$I_b = \frac{m_1 m_2}{m_1 + m_2} r^2 = \mu r^2 \tag{8}$$

and m_1 and m_2 are the masses of the atoms and μ is the reduced mass of the two atoms.

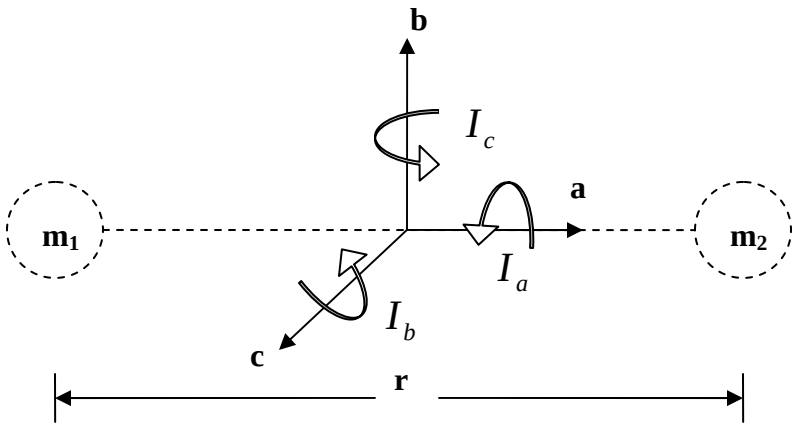

Figure 2-2 Rigid rotator

If we assume that the molecule is rigid system then there would be no potential energy associated with its rotation. The Schrödinger's equation for the system is

$$\nabla^2 \psi + \frac{8\pi^2 \mu}{h^2} E \psi = 0 \tag{9}$$

The eigenvalues of the energy E are

$$E = \frac{h^2}{8\pi^2 I} J\left(J+1\right) = BJ(J+1) \qquad (10)$$

where J is the rotational quantum number [21].

The quantum mechanical selection rule governing rotational transitions is $\Delta J = \pm 1$. Since transitions other than these two transitions are forbidden, anharmonicity is not observed in rotation [30]. Moreover, actual molecules are not rigid systems. In non-rigid bonding, the distance between the two atoms is not constant. The centrifugal force elongates the bond as the rotation velocity increases. Therefore, the moment of inertia is no longer constant. This effect can be seen as the distances between energy levels slowly decrease with increasing rotational quantum number [27]. To account for the non-rigid bonding effect, an extra term is added to equation 10

$$E = BJ\left(J+1\right) - D(J(J+1))^2 \qquad (11)$$

where D is the centrifugal distortion constant and depends on the moment of inertia and the elasticity of the bond [29].

2.4.2.3 Energy in molecules

The energy of a molecule is given as the sum of its translational, rotational, vibrational, and electronic energies. That is

$$E_{mol} = E_{trans} + E_{rot} + E_{vib} + E_{elect} \qquad (12)$$

Since E_{trans} has little effect on molecular spectra, it is disregarded here. In addition, E_{elect} is related to three kinds of electrons. One kind is the inner shell electrons which belong exclusively to a single atom, and have negligible contribution to E_{mol} and may be disregarded. The other two kinds of electrons which are shared electrons can be either shared by two adjacent atoms for one kind, or shared by more than two atoms for the other kind. These electrons are concerned with transitions between rotational and vibrational electronic energy levels when irradiated by ultraviolet or visible radiation.

Since IR radiation does not normally excite such transitions, E_{elect} will be disregarded. The E_{rot} term depends on the moments of inertia of the molecule and it is entirely kinetic. Molecular rotation in liquids and solids is normally hindered or prevented completely by intermolecular forces. Thus, E_{rot} primarily results from the freely rotating molecules in the vapor state [28]. Hence in this study one can reasonably reduce equation 12 to become

$$E_{mol} = E_{rot} + E_{vib} \qquad (13)$$

2.4.3 Origin of IR absorption spectra

IR absorption spectra are graphs of radiation intensity (absorbance) versus position (wavelength or wavenumber). Not all matter, metals for example, is capable of producing IR spectra. However, the compounds that are capable of producing IR spectra show a number of bands which supply the primary data for compound identification. The absorption bands on the spectrum of a compound come from the interaction of radiation with the vibrations and rotations of molecules [31].

2.4.3.1 Absorption

The transfer of energy from the incident radiation to matter, in which it results in increase of molecular motion, is referred to as absorption. The energy gained by the molecule from light absorption excites a quantized structure to a higher-energy state [32]. The wavelength of the absorbed radiation determines the location of the absorption band in the spectrum [31]. Since the molecule has vibrational and rotational motions, the absorption of radiation excites the molecule to a higher vibration-rotational energy state. The following two sub-sections will discuss the absorption process in the molecular vibration and rotation.

2.4.3.1.1 Absorption process in molecular vibration

In a molecule with unlike atoms, the electric charge distribution in the bond changes during vibration making the molecule behave like an oscillating dipole. For example, see the second mode of vibration in figure 2-1 in which the outer atoms move

antisymmetrically with respect to the central atom. This makes the charge distribution on one side of the linear molecule larger than the other side at one instant of time and then vice versa at another instant of time [22]. The varying electric field due to radiation interacts with the varying electric field due to vibration in the molecule in such a way that energy can be transferred from the radiation to the molecule if the frequencies are equal. This interaction cannot occur in molecules with no dipole moment [29]. Thus, permanent dipole is essential for strong IR absorption. However, symmetrical polyatomic molecules such as C_2H_2 do experience strong absorption. The reason for that is the individual bonds have dipole moments but, due to symmetry, the bond moments cancel each other making the molecule non-polar as a whole [25]. The molecular vibration determines the absorption frequency and the effectiveness of the energy transfer from the radiation to the molecule determines the absorption intensity and it depends on the change in the dipole moment that occurs during vibration [30].

2.4.3.1.2 Absorption process in molecular rotation

For a non-rotating molecule with a permanent dipole, the molecule will rotate to follow the alternation of the alternating electric field from the radiation just like an electric motor. When the molecule rotates in phase with the alternating electric field, energy can be transferred from the radiation to the molecule. For a rotating molecule with a permanent dipole, the electric field should have a frequency equal to the first of the quantized angular frequencies of the rotating molecule to ensure that they both move in phase all the time which will result in complete absorption. If the two frequencies are not equal, the two waves would be in phase during a certain period and out of phase for another which will result in incomplete energy transfer from the radiation to the molecule. This results in no absorption [33].

2.4.3.2 Vibration-Rotation spectra

The fact that molecules in gaseous state rotate freely, makes it possible for a change in the vibrational state to be accompanied by a change in the rotational state. Molecules at room temperature are distributed over a considerable number of rotational states, thus making it possible to have an increase in vibrational energy to be accompanied by

increase or decrease in rotational energy. Since the vibrational energies are on the order of a hundred times greater than the rotational energies [25], the interaction between the vibrational and rotational motions can be disregarded as a first approximation and the energy levels can be obtained by the summation of the energy levels of the vibration and rotation. This could be visualized as a superposition of the rotational energy levels and the vibrational energy levels, see figure 2-3.

Therefore equation 13 can be written as

$$E_{mol} = E_{vib} + E_{rot}$$

$$= \sum_i \left(n_i + \frac{1}{2} \right) h\nu_i - \left(n_i + \frac{1}{2} \right)^2 h\nu_i x_i + B_{vr} J(J+1) - D_{vr} J^2 (J+1)^2 \quad (14)$$

It should be noted that the constants B_{vr} and D_{vr} in the above equation are not the same as the ones in equation 11. This is because the average distance between the atoms increases with increasing vibration. Likewise, the centrifugal stretching changes with increasing vibration. The selection rules for the combined motions are $\Delta J = \pm 1$ and $\Delta n = \pm 1, 2 \ldots$ [27].

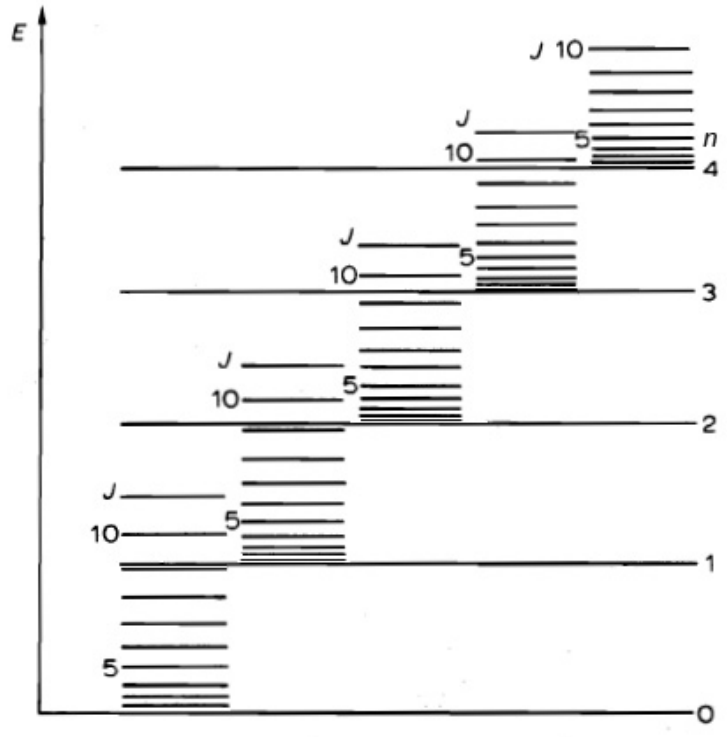

Figure 2-3 Superposition of vibrational and rotational energy levels [27]

The energy transitions in vibration are so large that, even at room temperature, most of the molecules are in the lowest vibrational state. This also gives the impression that the spectrum is determined by pure vibrational changes. However, the near-IR spectra of gases has a fixed position determined by the vibrational change and, because of the rotation motion effect, exhibits a structure consisting of a series of lines in two sets. The set of lines at the shorter wavelength originates from molecules whose rotational energy increases simultaneously with the increase in the vibrational energy (called R-branch) and those at longer wavelength from molecules whose rotational energy decreases as the vibrational energy increase (called P-branch). The two sets or branches are centered around a missing line called Q-branch, see figure 2-4. This figure represents a generic profile of the lines. The two branches are not always symmetric [25].

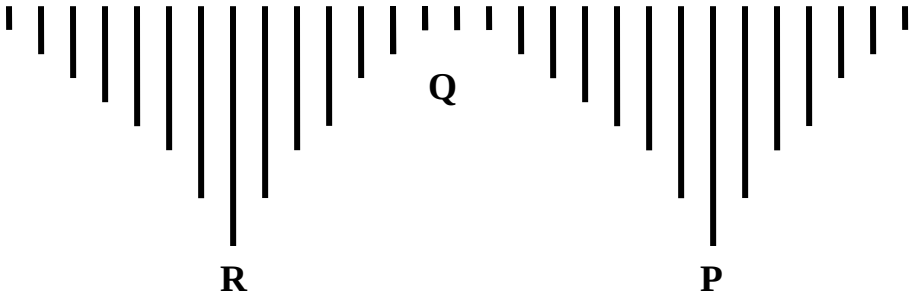

Figure 2-4 Absorption lines in near-IR spectra of gases

The relative intensities of the lines are related to the relative population level of the rotational level of the lower vibrational state which is related to the temperature, the magnitude of the rotational quantum and the degeneracy of the rotational level. Each line is labeled according to the rotational quantum number of the ground vibrational state. Therefore, the first line in the R-branch is labeled R(0) and the first line in the P-branch is labeled P(1). There is no P(0) due to the fact that the upper level cannot have -1 rotational quantum number, see figure 2-5 [29].

The dotted part of the vertical lines in figure 2-5 indicate the large distance between two vibrational levels compared to the spacing of the rotational levels. The (a) spectral lines show the lines location for the case of interaction between vibration and rotation and the (b) spectral lines show the lines location for the case of no interaction between the two motions [27].

For linear molecules with a center of symmetry such as C_2H_2, the IR spectrum shows a lines pattern of alternating intensities. This is because each of the rotational levels for which J is odd splits into 3 energy levels. The splitting of the rotational energy level has been traced back to the spin of nuclei in the molecule. Having degenerate energy levels increases the population of molecules in that level [29].

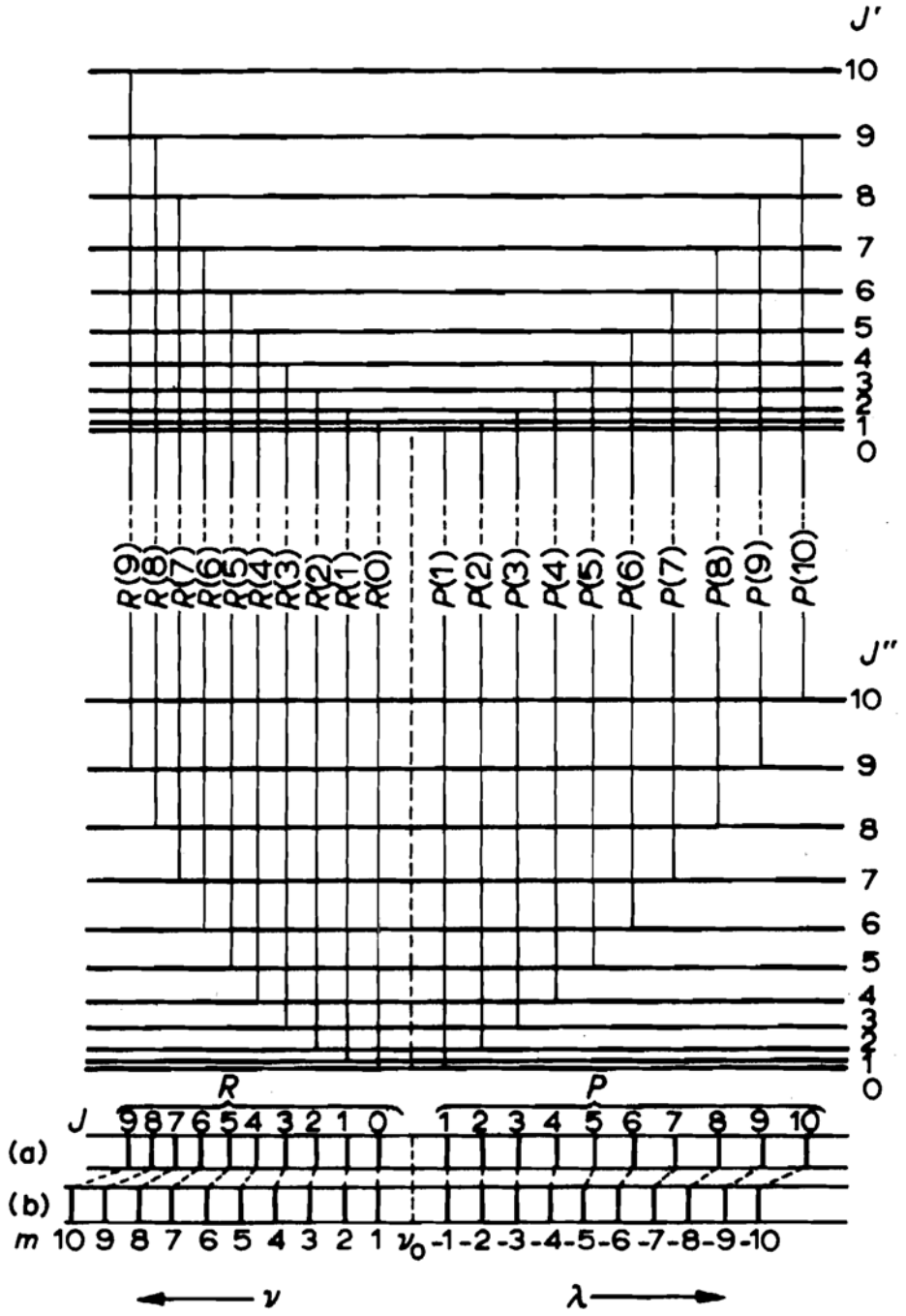

Figure 2-5 Energy level diagram showing the fine structure of the vibration-rotation band [27]

2.5 The basic principle of the sensor's operation

Since the spectroscopic techniques are being considered in the design, the operation of the near-IR sensor should follow the principles of an IR spectrometer. The sensor consists of an IR source, a gas cell, and an IR detector. An optical fiber, acting as a transmitter, delivers the IR radiation to the capillary tubing which serves as a gas cell. The light passes through the sample contained in the gas cell to another optical fiber, acting as a receiver, which delivers the altered IR radiation to the detector. See figure 2-6.

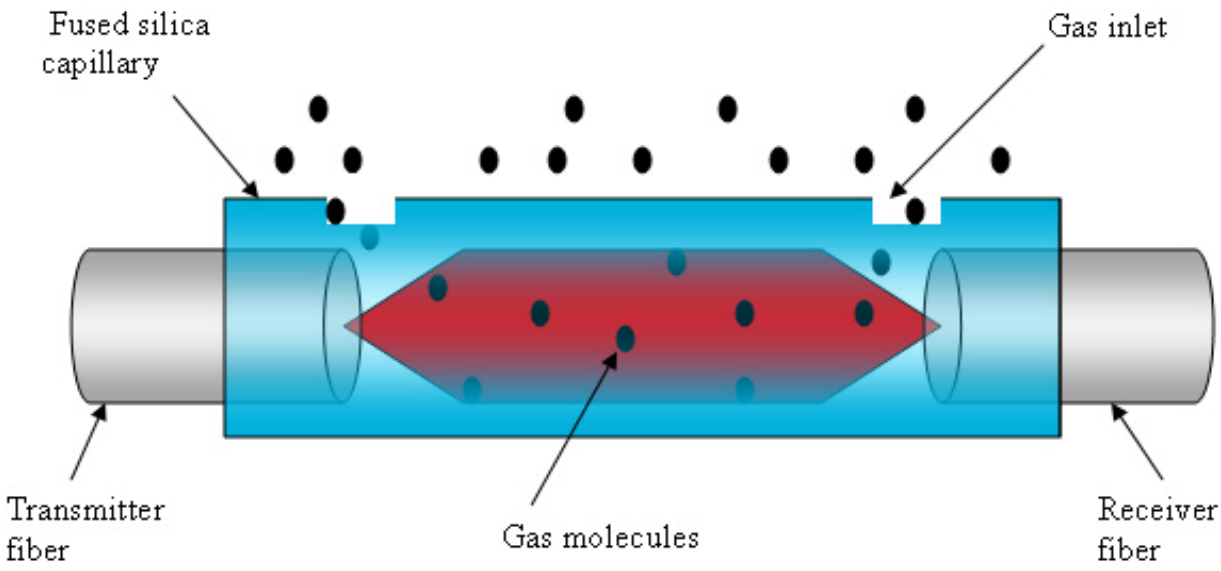

Figure 2-6 Near-IR gas sensor

The sensor can be either operated in transmission or reflection mode. In the reflection mode operation, a reflector at one end of the cell is needed to reflect the signal back to the optical fiber. The sensor can also be operated under either static or dynamic pressure and at temperatures just below the softening point of fused silica (1600 ºC) [34].

The optical interaction between the propagating light and the gas in the cell produces sharp absorption lines in the IR spectrum. These lines result from the overtones of the fundamental molecular vibrations of the gas molecules and are governed by the Beer-Lambert law. This law states that there is a direct and linear relationship among the radiation absorbed by the sample, the concentration of the desired species in the sample, and the path length of the sample [31]. In mathematical terms, this relation is expressed as

$$A = \varepsilon c l \tag{15}$$

where A is the absorbance of the sample, c is the concentration, l is the path length of the sample, and ε is a constant that depends on the absorptivity of the species at a particular wavelength. This law is based on two assumptions: the incident radiation is monochromatic and each absorbing center is independent of all others regardless of their kind or concentration [30].

2.5.1 Derivation of the Beer-Lambert law

The Beer-Lambert law can be derived, based on [29], from the following. Consider a light beam of specific wavelength passes through some material that contains absorbing centers. All absorbing centers of the same kind should absorb light at that wavelength to the same extent. Thus one should expect that the amount of light absorbed should be doubled by doubling the number of absorbing centers. Likewise, if we consider the material to consist of thin layers containing the same number of absorbing centers then each layer should absorb the same amount of light. However, since layers closer to the light source reduces the amount of light energy incident on layers further from the source, the amount of light energy absorbed by each layer is actually not the same. Let there be n number of layers, and each have an arbitrary thickness l_o . The total path length through the sample is

$$l = n l_o \tag{16}$$

The light emerging from the ith layer has an intensity of I_i and is a fraction f of the light intensity incident on that layer, which is the light emerging from the (i-1)th layer.

$$I_i = f I_{(i-1)} \tag{17}$$

Thus the intensity of light transmitted through the whole sample is given by

$$I_n = f I_{(n-1)} = f^2 I_{(n-2)} = \ldots = f^n I_o \tag{18}$$

where I_o is the light intensity incident on the sample. By rearranging the terms and taking logs of both sides of equation 18 we get

$$\log_{10}\left(\frac{I_o}{I_n}\right) = n\log_{10}(f) \tag{19}$$

Dividing the path length and multiplying the concentration c by two does not change the number of absorbing centers in the path of the light. Therefore, for a fixed path length, the variation of n with concentration and layer thickness can be expressed by

$$n = \frac{cl}{c_o l_o} \tag{20}$$

where c_o is a standard concentration. Substituting equation 20 into equation 19 gives

$$\log_{10}\left(\frac{I_o}{I_n}\right) = \frac{cl}{c_o l_o}\log_{10}(f) \tag{21}$$

The left side of equation 21 is defined as the absorbance, A. The constant term in the right side, $\frac{\log_{10}(f)}{c_o l_o}$ is called the absorptivity coefficient and is assigned the symbol ε.

This makes equation 21 look exactly like equation 15.

The radiation energy that passes through the sample has three components. Some of the light will get transmitted, some will get reflected, and some will get scattered. As one can see from figure 2-7, the transmitted energy is then reduced by the other two components. Therefore, the transmitted light depends on the absorption of the gas as well as the reflectance and scattering power. To account for these two components, equation 15 can be rewritten as

$$\log_{10}\left(\frac{I_o - R - S}{I_n}\right) = \varepsilon cl \tag{22}$$

where R is the reflection component and S is the scattering component [20].

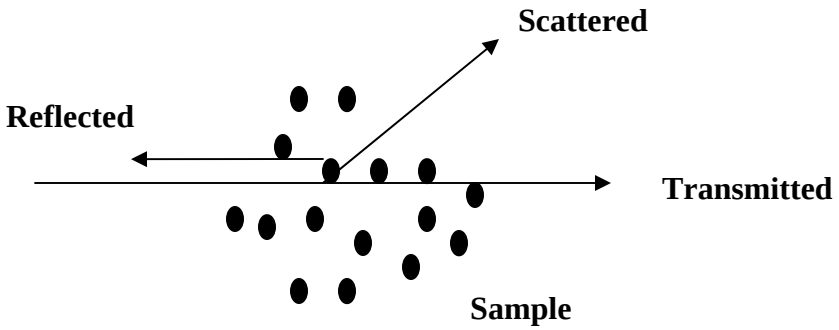

Figure 2-7 Radiation components as it passes through the sample

From the Beer-Lambert law one can conclude that the sensing capabilities (single gas detection) of this sensor can be maximized by using:

1) A narrow-linewidth source centered on a relatively strong absorption line to ensure a large value for the absorptivity coefficient.
2) A long effective path length.
3) Signal processing techniques to improve signal-to-noise (S/N) ratios. That is, to increase the ability to detect a very small intensity change [18]

Chapter 3: The Acetylene molecule

Since we are concerned with the acetylene gas, the acetylene molecule will be examined. Here we will identify the significance of the acetylene gas, its chemical and physical properties, its molecular structure, and its near-IR spectrum.

3.1 Acetylene

According to the chemical hazards guide of the National Institute for Occupational Safety and Health the chemical compound Acetylene with its chemical formula C_2H_2 is a colorless and extremely flammable gas at standard temperature and pressure. It normally has a faint, ethereal odor. However, the commercial grade, which is shipped under pressure dissolved in acetone, has a garlic-like odor. Acetylene forms explosive acetylide compounds with copper, mercury, silver & brasses. Upon exposure, it targets organs such as the central nervous system and the respiratory system and causes symptoms such as headache, dizziness, and asphyxia. Acetylene is mainly used for welding and cutting of metals and in chemical synthesis [35].

Although acetylene was discovered in 1836, the naturally occurring acetylene was not discovered until 1892 [36]. Being produced by human activities and some natural processes in seawater, it has been found to exist in the terrestrial troposphere. Further, the concentration of acetylene as a pollutant has been increasing for the past years in the urban and industrial environments [37].

3.2 The Acetylene molecule

According to the valence bond theory, the bonding of atoms in a molecule forms when the atomic orbitals overlap. The more they overlap, the stronger the bond. End on overlapping forms σ-bond (See figure 3-1) and sideways overlapping forms π-bond (See figure 3-2) [38]. The linear structure of the acetylene molecule in figure 3-1 forms from the overlapping of sp orbitals of the C atoms and the C atoms with the orbitals of the H atoms. The overlap of half-filled 2p orbitals in the two C atoms forms two parallel segments. When four of these segments exist, they merge into a hollow and symmetric

cylindrical shell as shown in figure 3-2. Thus, the final molecule structure would look like the structure shown in figure 3-3 [39].

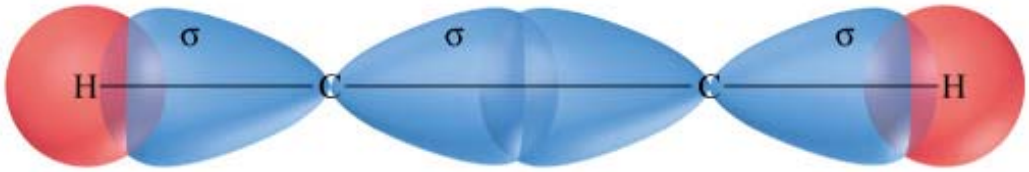

Figure 3-1 The σ-bond Framework [39]

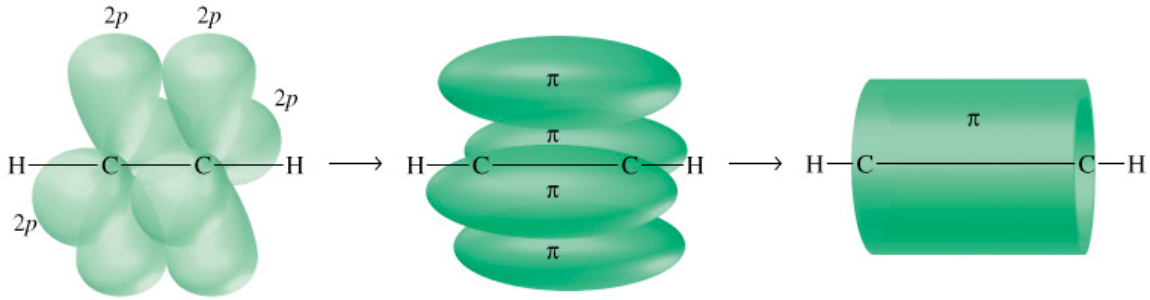

Figure 3-2 Formation of π-bonds by the overlap of half-filled 2p orbitals [39]

Figure 3-3 Acetylene Molecular Structure, modified from [39]

3.3 Acetylene's near-IR spectrum

Acetylene has absorption spectrum at different regions of the IR (See figure 3-4). Absorptions in the 4 to 5 μm range originate from the stretching vibration of the carbon triple-bonded C≡C. Whereas, absorptions in the 3.02 to 3.12 μm range originate from the

stretching vibration of the carbon hydrogen bond ≡C-H. The bending vibration of ≡C-H gives rise to absorptions in the 14.29 to 16.67 μm range. The 3.0 μm absorption band has an overtone at 1.5 μm region [40]. The absorption lines around the 1.5 μm region are attributed to the first overtone transition of the vibration-rotation spectra of H-C≡C-H molecules [41].

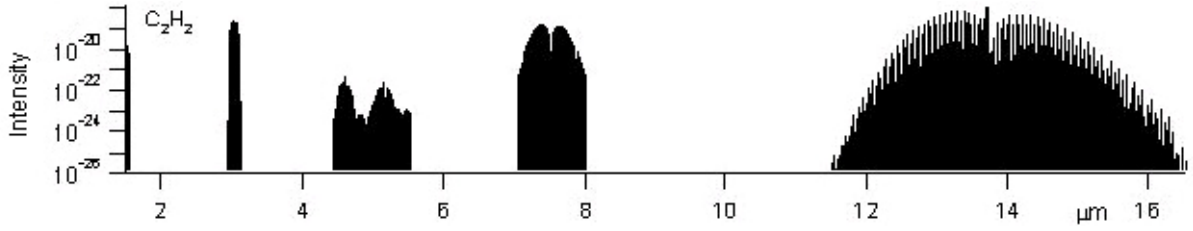

Figure 3-4 HITRAN's IR absorption spectra of acetylene [42]

Figure 3-5 shows the acetylene spectrum of the first overtone transition. The set of absorption lines around 1.52 belongs to the R-branch and the set of absorption lines around 1.53 belongs to the P-branch of the vibration-rotation modes.

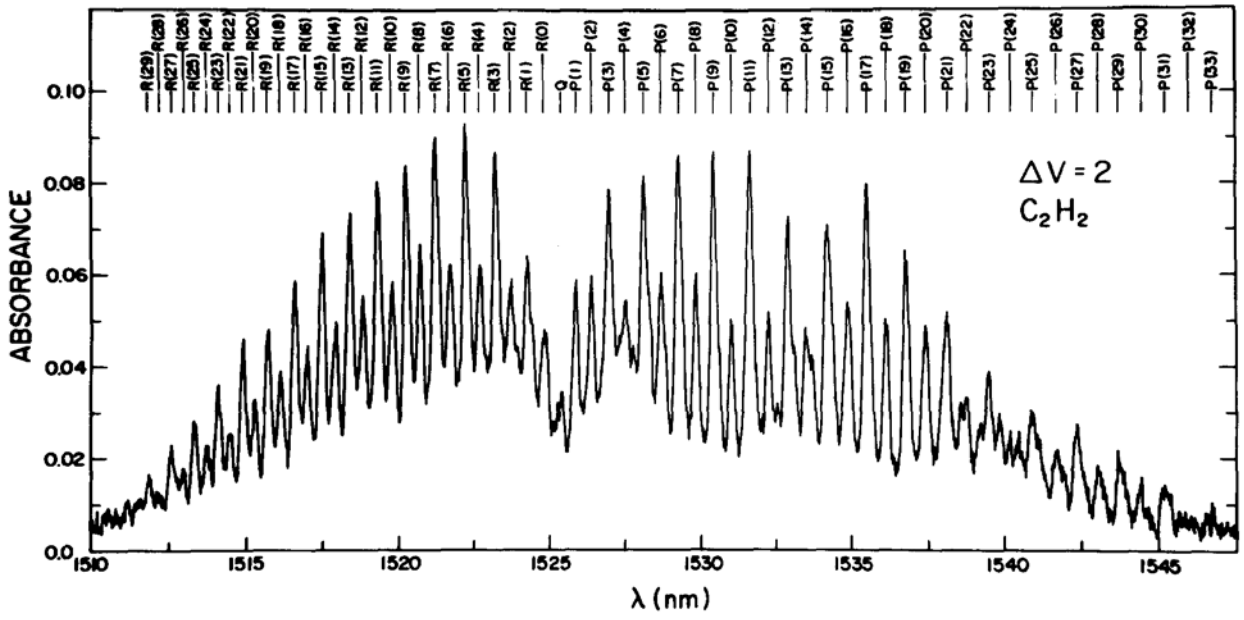

Figure 3-5 Acetylene spectrum of the first overtone transition [43]

The theoretical spectrum for acetylene can be generated using parameters acquired from the HITRAN database (See figure 3-7 on page 45). The original HITRAN data came

mainly from the experimental and theoretical work accumulated from 1973 to 2004. The HITRAN molecular spectroscopic database has been recognized as the international standard for providing the necessary fundamental spectroscopic parameters for diverse atmospheric and laboratory transmission and radiance calculations. The line positions in the HITRAN database are given in vacuum wavenumber (cm^{-1}). The units for intensity are cm^{-1} / (molecule × cm^{-2}) at the standard HITRAN temperature of 296 K. The data is based on a 31 cm path length and gas pressure of 0.5 Torr in vacuum [37]. The following equation is used to convert between wavenumber and wavelength.

$$Wavenumber\,(cm^{-1}) = \frac{10^4}{\lambda(\mu m)} \qquad (23)$$

By comparing the P and R branches of the two spectrums in figures 3-5 and 3-7 one can see that they both have the same absorption lines profile. This theoretical spectrum is in good agreement with the well known acetylene spectrum.

An actual acetylene spectrum of the sensor under study is shown in figure 3-6.

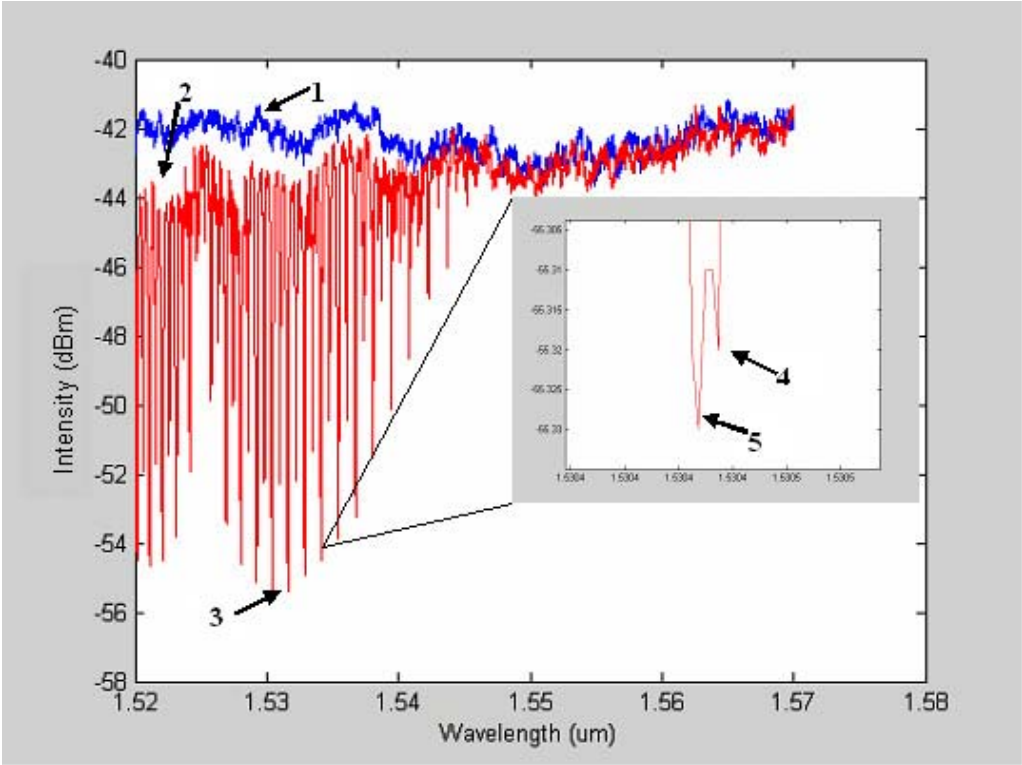

Figure 3-6 The sensor's acetylene spectrum

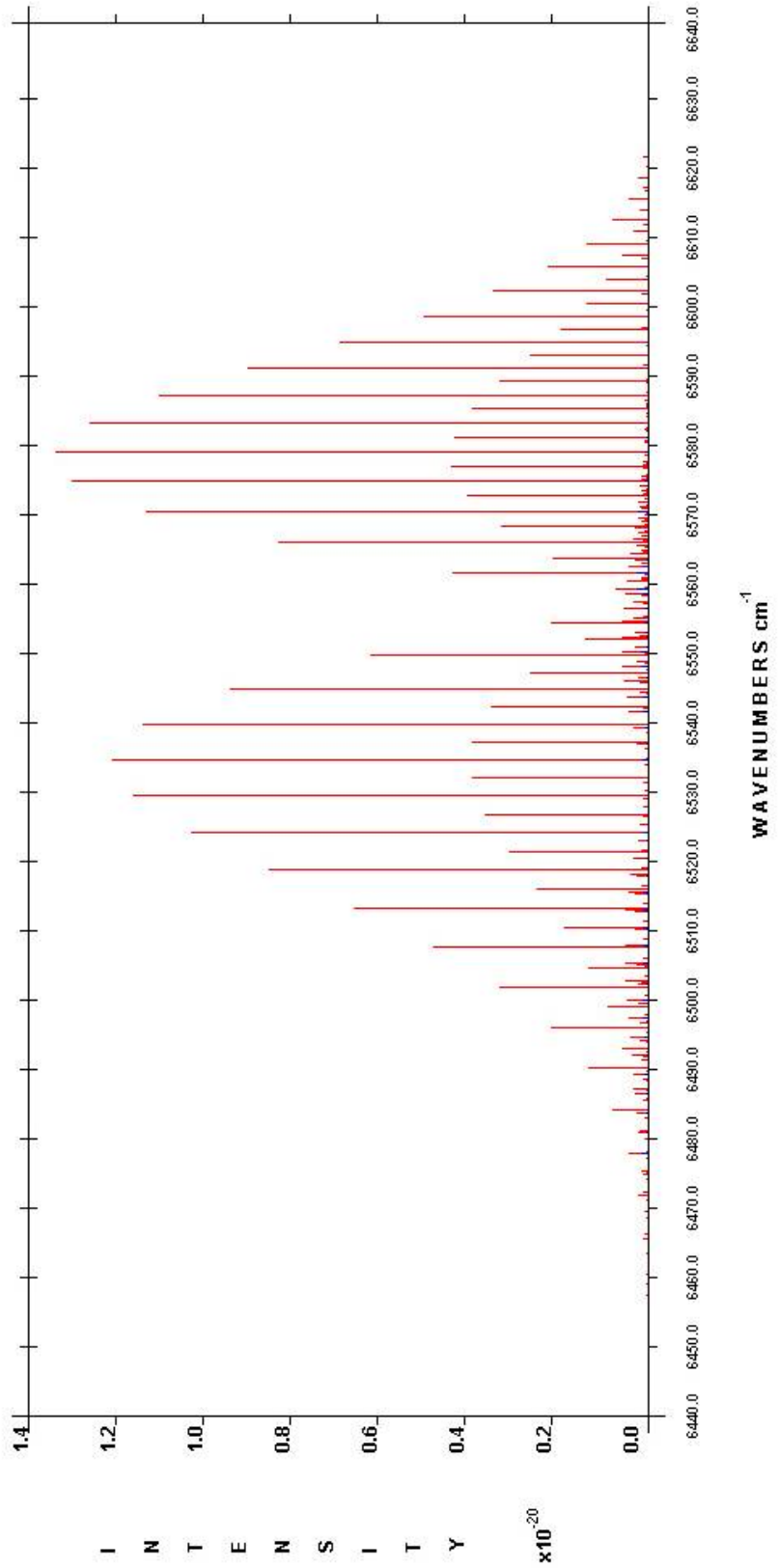

Figure 3-7 HITRAN's theoretical spectrum for acetylene

Figure 3-6 has the same absorption lines profile as figures 3-5 and 3-7. It shows good agreement with the theoretical and well known acetylene spectrum. It also shows features that are common in IR spectra. These features are:

1) Baseline
2) Area between baseline and transmitted light line representing background absorption or reflection losses
3) Absorption maximum of the vibration-rotation lines representing the maximum uptake of radiation energy by the acetylene molecules
4) $^{13}C_2H_2$ isotope maxima (isotope effect)
5) $^{12}C_2H_2$ isotope maxima (isotope effect)

Features 4 and 5 represent the separation of the line's maximum into two maxima. This phenomenon is explained by the isotope effect. The shift of maximum line position is due to the fact that the two isotopes have two different masses. The simultaneous presence of acetylene isotopes gives rise to the splitting of the line maximum [21]. Commercial acetylene contains 97.76% $^{12}C_2H_2$ and 2.20% $^{13}C_2H_2$ [37].

Chapter 4: Experimental results

In this chapter, the sensor under study is examined by direct observation. The data reported in this chapter will be analyzed in the data analysis chapter. First we will investigate the sensor's gas cell and its waveguiding behavior. Second, we will study the transmission and reflection of light through the gas cell. Third, we will examine the sensor's response as a function of physical dimensions and pressure. Then at the end, we will measure the sensor's response time.

4.1 The sensor's gas cell waveguiding characteristics

The sensor's gas cell is made of flexible fused silica capillary. The capillary tubing is synthesized, by Polymicro Technologies LLC, from purified silica. The tubing is also coated with polymer (standard Polyimide coating) to yield durable, strong, and yet flexible tube. This capillary has superior temperature resistance, high dielectric strength (very high breakdown voltage), and inert surfaces. These features make this material ideal for sensing in harsh environments. The tube's inner diameter (ID) ranges from 1 μm to 2 mm. The outer diameter (OD) of the tube ranges from 90 μm to 3.5 mm. The capillary tubing has been used in many applications such as analytical chemistry, gas and fluid delivery, flow cell and as a waveguide [34].

To investigate the capillary tubing waveguiding behavior, a 300 mm long tube with 134 μm ID was selected for two reasons. The tube's ID, or bore size, needed to be big enough to house a standard single mode optical fiber (SMF) and to allow reasonable gas flow throughout the tube. For IR radiation source and detection, a high-resolution swept laser interrogator system from Micron Optics Inc. was used. The system contains a fiber ring laser that is continuously swept from 1520 to 1570 nm and has dynamic range detection capability of more than 60 dBm. A preliminary investigation could be carried out by transmitting IR radiation in a straight line through standard single mode fiber, the capillary tubing, and free space. This comparison should show the transmission characteristics of the tube compared to the other transmission media. In the case of free space transmission, IR radiation from the laser source was coupled into an SMF, which was placed in line-of-sight with another SMF connected to the detector. As the light exits

the source fiber, it propagates in free space and then gets collected by the detector fiber. For the capillary case, the same source and detector fibers were inserted in the tube. Therefore, the light propagates in the tube. Finally, the two fibers were fusion spliced with a third SMF piece which makes the light propagate in the SMF. For all cases, the optical path length between the source and detector was 300mm. For fair comparison, the fiber and the tube were setup in a straight line configuration since light in free space travels in a straight line. The results are shown in figure 4-1.

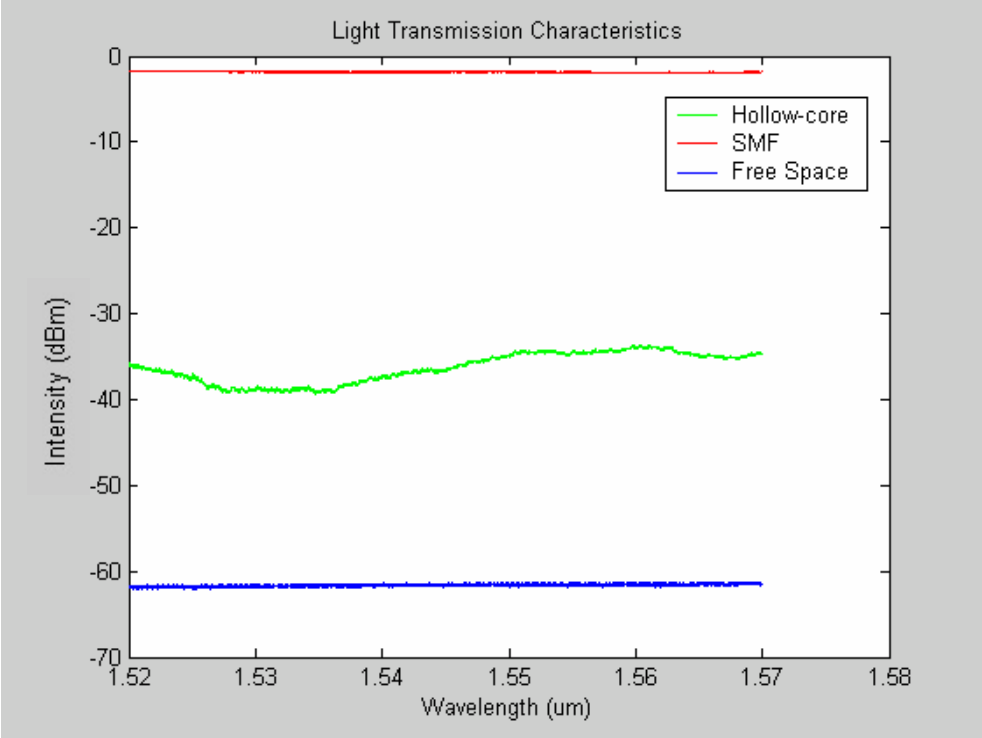

Figure 4-1 Transmission Characteristics in free space, SMF, and fused silica tube at 300mm path length

The blue spectrum represents transmission through free space, the green spectrum represents transmission through capillary, and the red spectrum represents transmission through SMF. Since capillary tubing suffers bending loss, it should be noted that only for the results reported in figure 4-1, the investigator tried to his best ability to setup the tube in the best possible straight line configuration. Thus, all other transmission data have loss variation due to poor bending loss control. Further, the loss in the tube at different path lengths was measured as shown in figure 4-2. The various path lengths were obtained by

varying the distance between the source and detector fibers. The black, red, green and blue spectra represent transmission through 300, 270, 250 and 150 mm path lengths respectively.

The capillary tube waveguide has a very small acceptance angle. The primitive coupling of light into the waveguide results in large variation in wavelength attenuation. A small change in the position of the source fiber could result in attenuation in specific regions of the spectrum or sometimes the entire spectrum. Figure 4-2 demonstrates this phenomenon. Also, small change in the detector fiber position will vary the coupling of the light from the waveguide to the optical fiber.

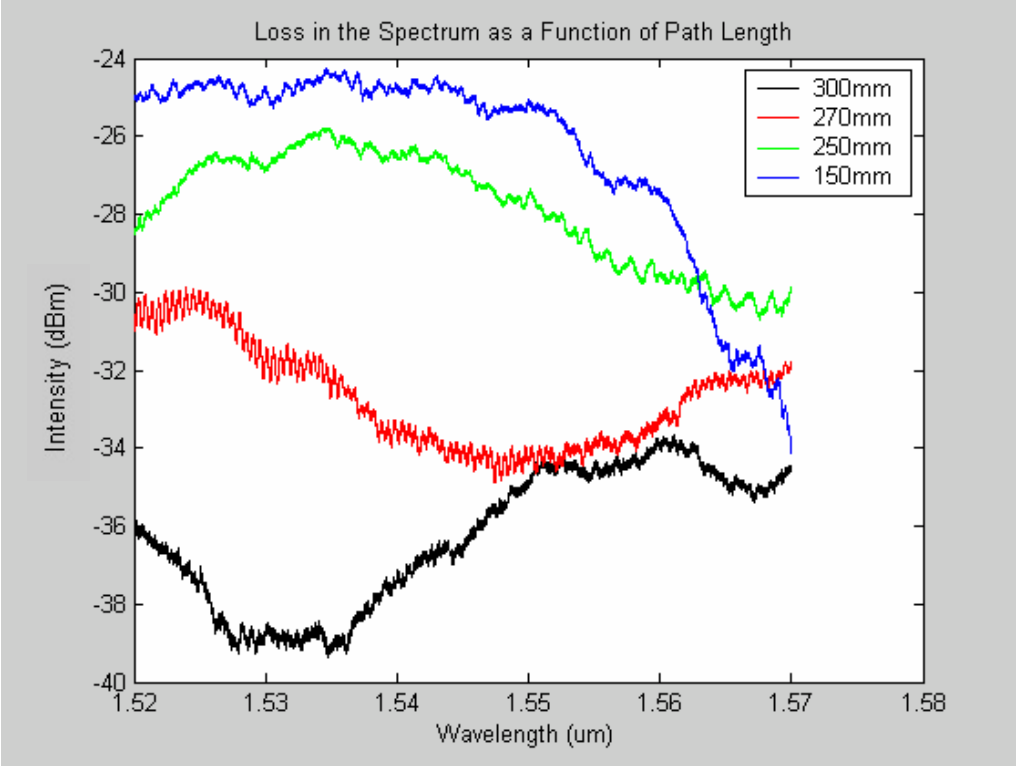

Figure 4-2 Loss in the Spectrum as a Function of Path Length

The openings in the tube which are needed to make the gas flow in and out the gas cell necessitated the study of its effect on the waveguiding characteristics of the tube. Therefore, the transmission study of the capillary was repeated but this time with a tube that has two holes in it. The source and detector fibers were placed before the holes, at the holes and after the holes as shown in figure 4-3. The results are reported in figure 4-4.

The blue, red, and green spectra represent transmission when the source/detector fibers are before, at and after the holes.

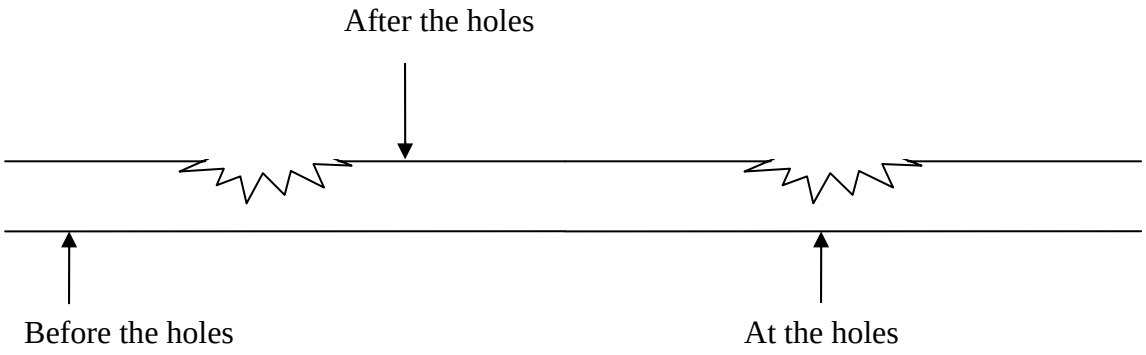

Figure 4-3 Source/Detector Fibers Positions Relative to the Holes

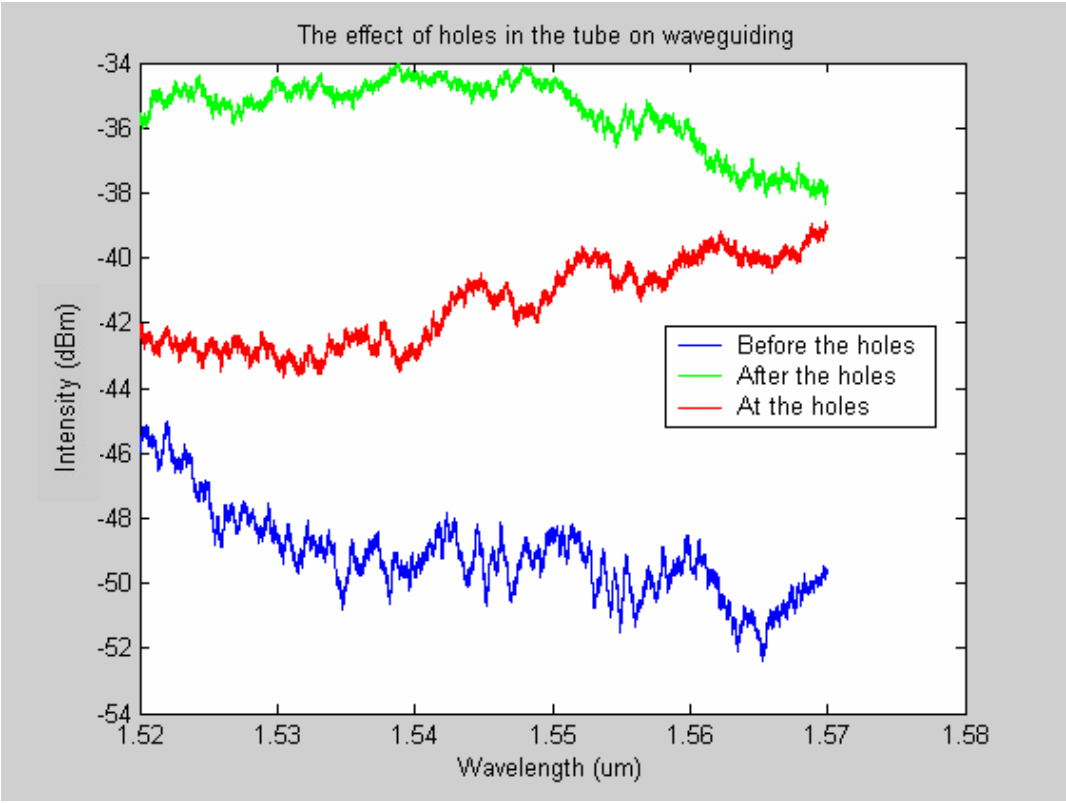

Figure 4-4 The Effect of Holes in the Tube on its Waveguiding Characteristics

4.2 Sensor fabrication and experimental setup

The sensors were fabricated by using a hollow fused silica tube (362 µm OD and 134 µm ID) from Polymicro Technologies, LLC, and two SMF-28 single-mode fibers with a 125 µm OD from Corning, Inc. An opening on the surface at the middle of the tube was made for the gas to flow in and out the capillary. A mid-range 50 mJ Excimer Laser MSX-250 from MPB Technologies Inc. was used to plunge a hole in the tube.

The experimental setup consists of an assembly of stainless-steel pipes connected through valves to an acetylene gas tank and a vacuum pump as shown in figure 4-5.

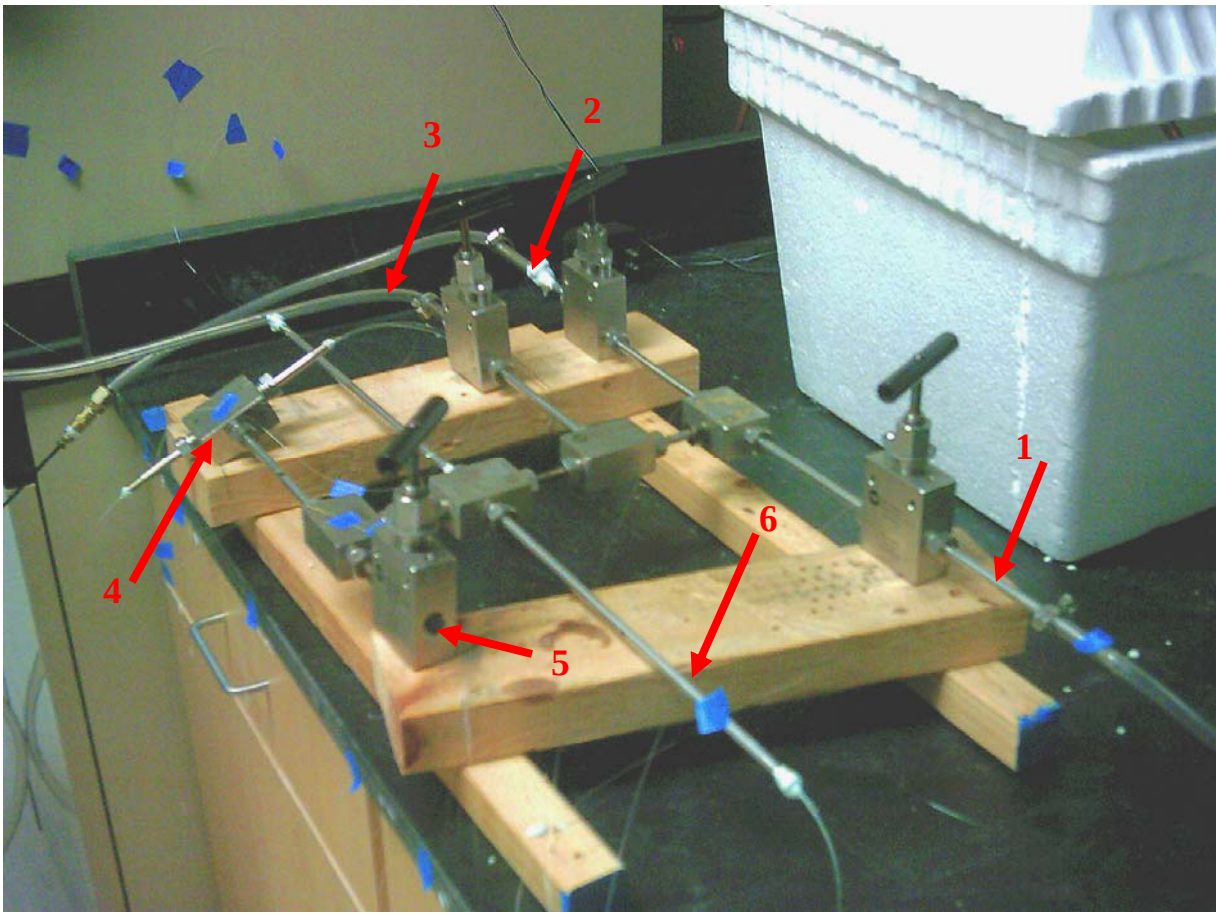

Figure 4-5 Experimental setup

The numbers on the figure represent the following:

1) To vacuum pump
2) To pressure gauge
3) To acetylene gas tank
4) Short path length sensors compartment
5) Exhaust outlet
6) Long path length sensors compartment

The sensors were installed and sealed with epoxy. Before starting the experiment, the setup was evacuated using the vacuum pump and then filled with acetylene to the desired pressure. Since acetylene is a flammable gas, the gas needs to be purged out before starting the evacuation process gain. This needs to be done to avoid damaging the vacuum pump. The experimental setup was configured so that all sensors will be tested under the same conditions.

4.3 Transmission vs. reflection mode

By far the main obstacle to decrease the sensor dimensions is the optical path length. In theory, an optical path length of a sensor operating in the transmission mode could be shortened by at least half by operating the sensor in the reflection mode. As the light passes the sample more than one time it results in an effective path length longer than the physical path length. Reflection mode sensors with different optical path lengths were fabricated as shown in figure 4-5.

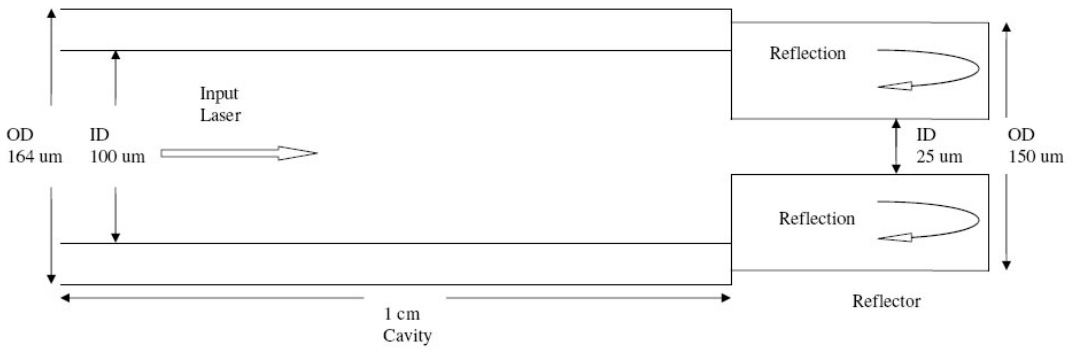

Figure 4-5 Reflection mode sensor

As the input radiation from SMF travels through the cavity it will get reflected by the end mirror of the reflector. The reflector is simply a cleaved surface of smaller inner diameter fused silica capillary tubing. The two tubes are bonded by fusion splicing. The splicing point was tested after splicing to ensure that the tubes didn't collapse. This ensures that the gas flows in and out of the cavity freely.

Sensors with 2, 5 and 10 mm path lengths were tested. All sensors responded in a similar manner. For example, the response signals of the 5 mm path length sensors, one operating in transmission and other in reflection, were measured simultaneously at 20 Psi and room temperature and recorded in figure 4-6.

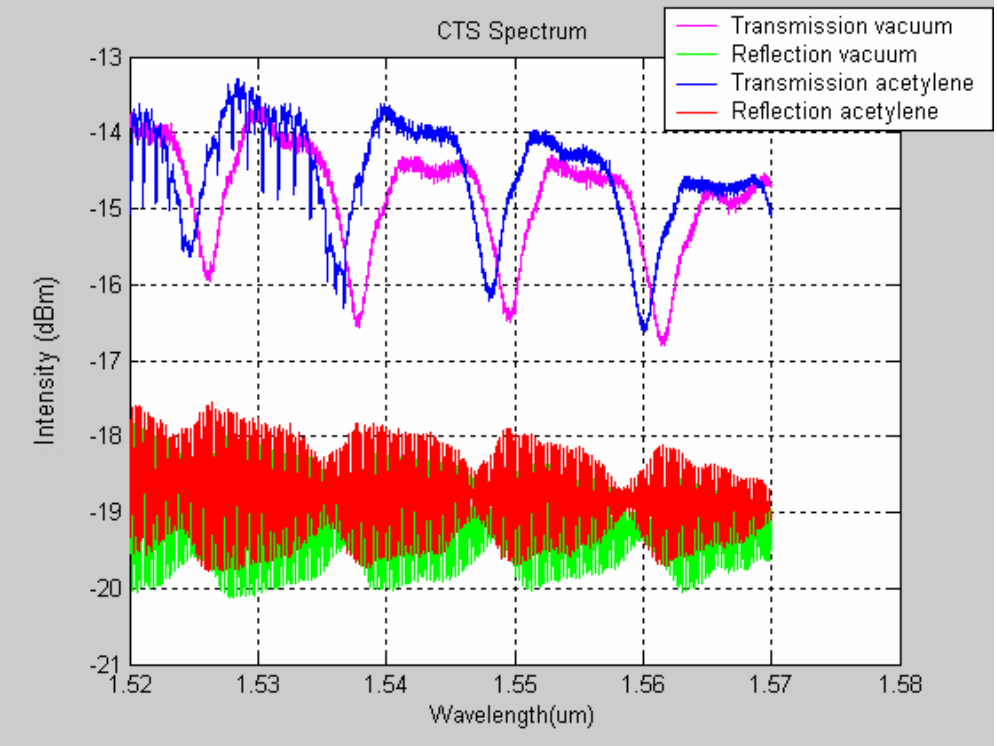

Figure 4-6 Transmission vs. reflection mode response signals

Figure 4-6 clearly demonstrates that absorption lines are not visible in the response signal of the reflection mode sensor. However, coating the reflector surface with good reflecting material, also use antireflection materials on the SMF surface to reduce multiple reflections in the cavity, and using signal processing techniques should improve the response signal of the sensor operating in the reflection mode.

4.4 Optical path length

In this section, the sensor's response as a function of optical path length was examined. Nine sensors with path lengths ranging from 125 μm to 250 mm were fabricated and tested in the same gas chamber at the same static pressure and temperature. To do so, the sensors were installed and sealed in a gas chamber. The chamber was evacuated for 3 minutes and then filled with acetylene under a static pressure of 20 Psi and at room temperature. For consistency purposes, odd number absorption lines of the P-branch that are labeled from P(1) to P(19) were used to report the results in figure 4-7. Each data point in the figure represents the average intensity of the selected 10 absorption lines, P(1) to P(19). The data shows no absorption lines for path lengths below 0.5mm for this particular setup. The 1 mm path length sensor showed an average intensity of about 0.18 dBm whereas the 250 mm path length sensor showed an average intensity of 21.6 dBm. It should be noted that in order to have figures 4-7, 4-8, 4-9, 4-10, 4-12, and 4-13 in this presentation the absolute value of the y-axis values where used.

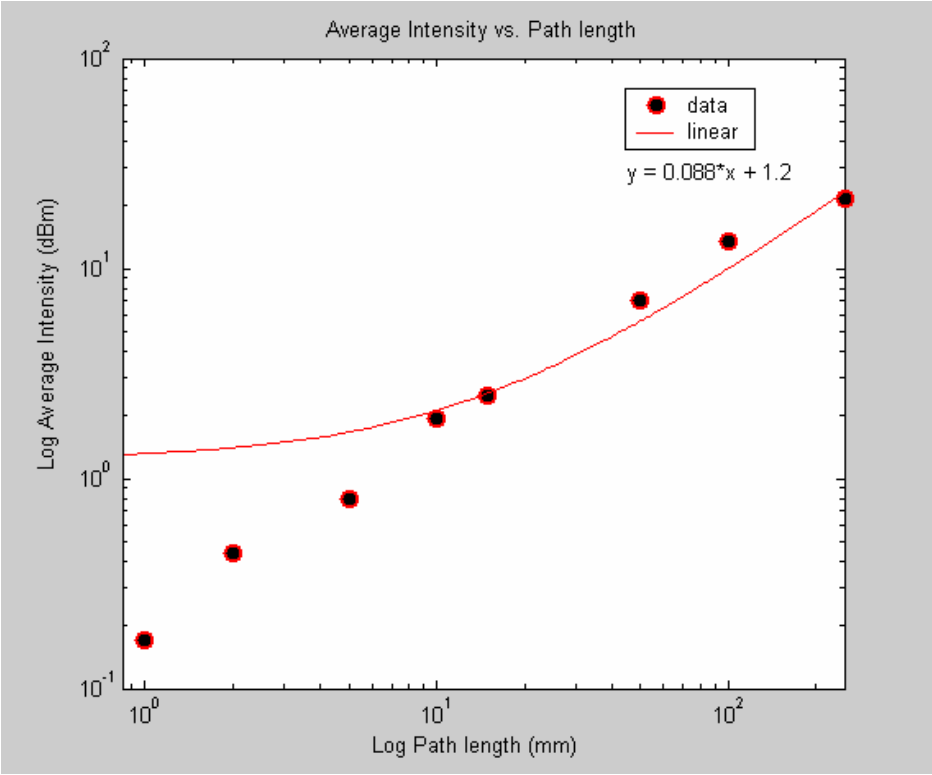

Figure 4-7 Average Intensity vs. Path length at 20 Psi [44]

4.5 Bore size

To determine the effect of the bore size on the sensor's response, five sensors with the same optical path length of 50 mm and bore size ranging from 2 μm to 134 μm were fabricated and tested in the same gas chamber under a static pressure of 10 Psi and at room temperature. Similar to the optical path length experiment, the odd number lines from P(1) to P(19) were measured in each of the five sensors spectra and then averaged. The results are shown in figure 4-8.

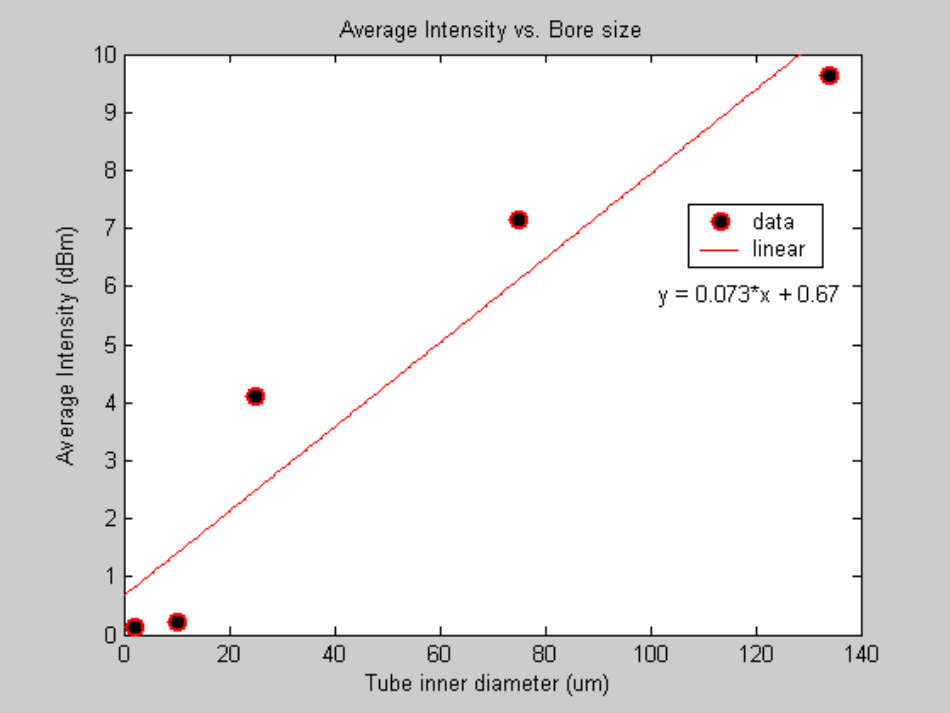

Figure 4-8 Average Intensity vs. Bore size at 10 Psi [44]

4.6 Pressure

The effect of pressure of the sensor's response was also examined. For comparison purposes, the 250 mm and the 1 mm path length sensors were tested under different levels of applied pressure at room temperature. The cell was tightly sealed to keep a constant pressure. Figures 4-9 and 4-10 demonstrate the effect of pressure on absorption for 250 mm and 1 mm path lengths respectively.

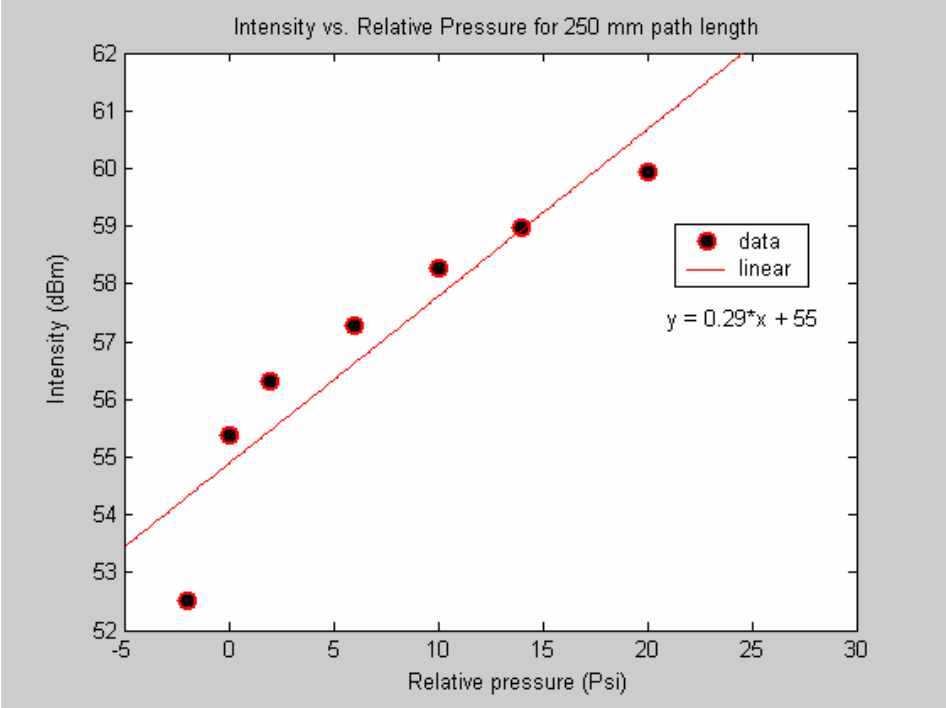

Figure 4-9 Intensity vs. Pressure for 250mm path length

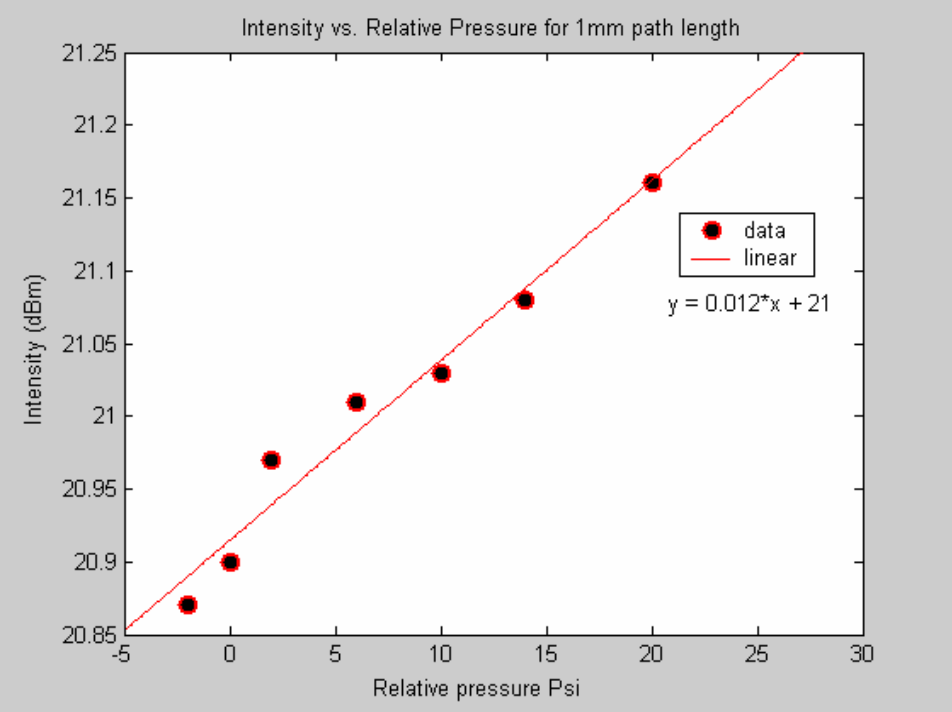

Figure 4-10 Intensity vs. Pressure for 1mm path length

Moreover, superimposing spectra of different pressure levels and then zooming in at any of the absorption lines shows pressure broadening effect. The broadening of absorption lines in a spectrum occurs as a result of collisions between excited molecules [45]. Pressure broadening, also known as collision broadening, is demonstrated in figure 4-11. In this figure, the red, green and blue lines represent spectra at pressure levels: below atmospheric pressure, at atmospheric pressure, and 5 Psi respectively.

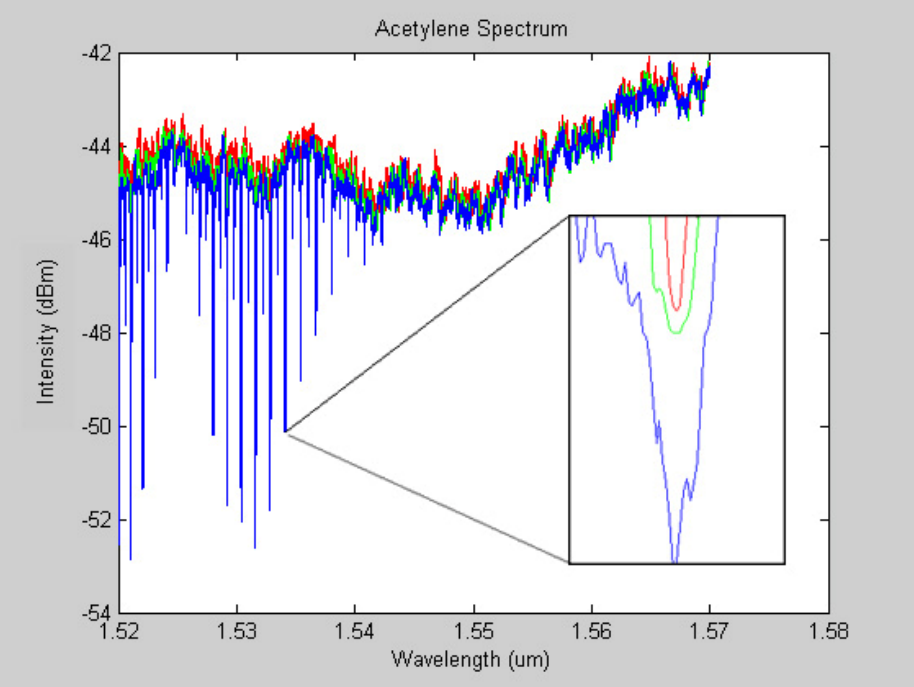

Figure 4-11 Pressure Broadening

4.7 Response time

The 250 mm and the 1 mm path length sensor discussed above were also used to measure the sensor's response time. The decay curves shown in figures 4-12 and 4-13 correspond to diffusion of the acetylene gas out of the two holes in the 250 mm hollow waveguide and out of one hole in the 1 mm waveguide. The measurement was done by purging the gas and collecting spectra data at timed intervals. The response time measurement is limited by the time required to open the gas valve and acquire the transmission signal. It takes at least 10 seconds for the operator to open the valve and start taking snap shots of the spectrum. The absorption line intensity drops as soon as the gas starts to flow out of the gas cell. Since the gas is under pressure, the flow rate decays exponentially with time

as the pressure in the gas cell gets equalized. Thus, the measurement should have a fast component corresponding to the fast flow rate when gas is first released and a slower component corresponding to the slower flow rate when the pressure reaches equilibrium.

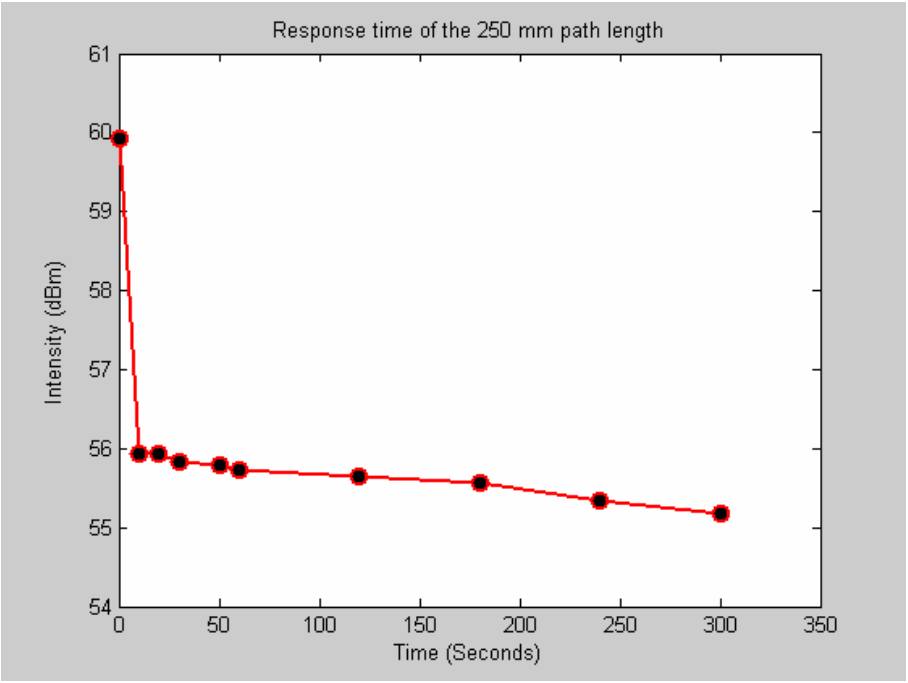

Figure 4-12 250mm Path Length Response time

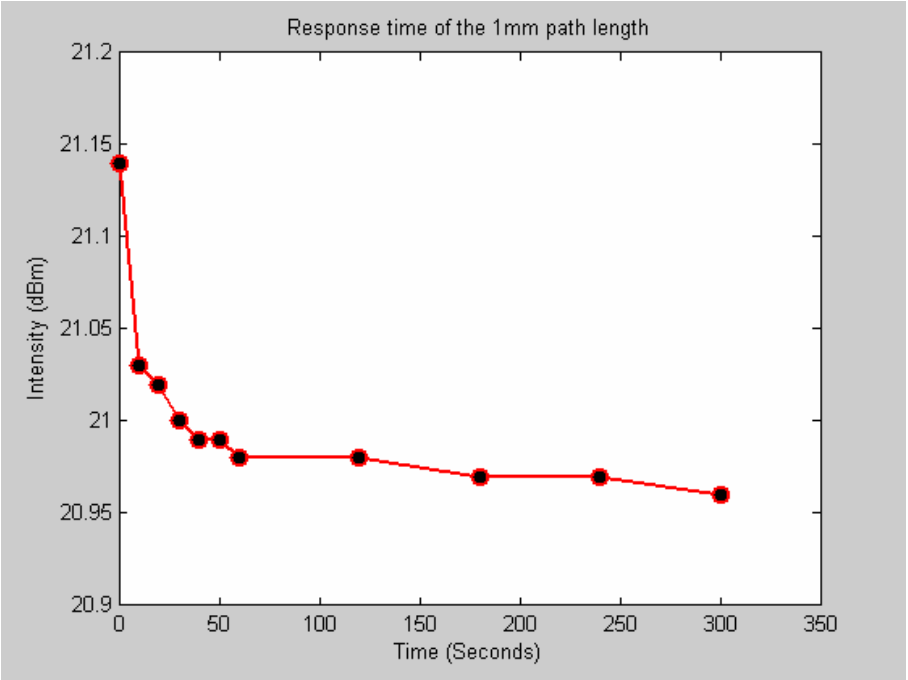

Figure 4-13 1mm Path Length Response time

Chapter 5: Data Analysis

The data reported in chapter 4 will be analyzed here. Also, the miniaturization of the sensor will be discussed. First we will demonstrate the capillary's ability to guide light. Second, we will analyze the pressure effect on the sensor's performance and the possibility of estimating pressure information. Third, we will discuss the response time and the detection limits of the sensor. Then at the end, we will establish the optimum dimensions to produce the smallest possible miniature sensor.

5.1 Capillary tubing as a waveguide

The results in figure 4-1 show that the capillary does guide light as it passes through it. Further, Figure 4-2 also shows typical waveguide characteristics in which the loss varies linearly with the length of the waveguide. According to Polymicro the refractive index of the synthetic fused silica at wavelengths in the range of 1.5 μm is n_2 = 1.44 [34]. Since the capillary is hollow, the refractive index of the core is that of the gas passing through it, which for most gases are near n_1 =1 [46]. Figure 5-1 shows the refractive index profile of the hollow waveguide. In the n_2 region there exist bound or surface wave modes. However, these modes get attenuated by the material. Thus, we regard the modes that propagate within the hollow core as leaky modes.

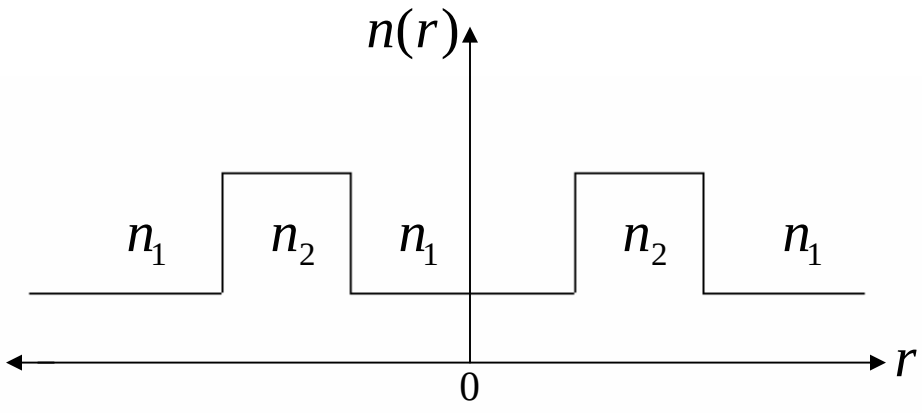

Figure 5-1 Hollow waveguide refractive index profile

It has been shown by Miyagi and Nishida that the attenuation constants are proportional to $\frac{\lambda^3}{r^4}$ where r is the inner radius of the hollow waveguide. Choosing a large bore size relative to the wavelength decreases the losses in the waveguide. The data in 4-8 supports this theory [47].

The wave optic theory of transmission through a dielectric hollow waveguide describes the total transmission loss as

$$Loss_{tot} = \left(\frac{\alpha}{a^3}\right) l_{tot} + \left(\frac{m}{R}\right) l_{bend} \qquad (23)$$

where l_{tot} is the total length of the waveguide and l_{bend} is the length of the bent portion of the waveguide. α and m are constants that depend on wavelength, index of refraction and the surface roughness of the waveguide, and optical modes of the transmitted light. The power coupling from the transmitted modes to the propagating modes of the receiving fiber also contribute to transmission loss. Therefore, we have in contrast to the solid-core fibers, a loss that depends strongly on the bore size, propagating modes, and bending radius of the waveguide [48].

The large variation in wavelength attenuation in the reported result is attributed to the large variation in the positions transmitter and receiver fibers inside the tube. In the processes of fixing the fibers in position, it's difficult to control the position of the fibers inside the tube since the fiber's OD is smaller than the tube's ID, (See figure 5-2).

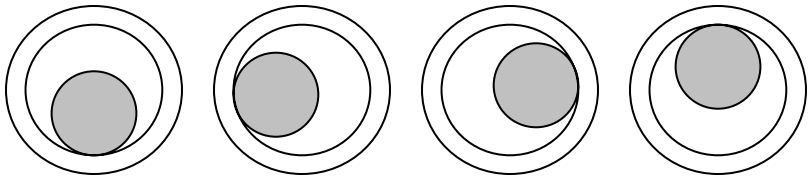

Figure 5-2 Fibers positions inside the capillary tube

Different positions excite different modes. The higher-order modes can be strongly attenuated by the hollow waveguide. It has been reported that hollow waveguides tend to attenuate higher-order modes and thus, have been shown to deliver nearly single-mode

light [49]. In addition, higher-order modes will not be coupled to the receiving fiber. This explains the large variation in wavelength attenuation due to poor coupling of light into the fiber.

Figure 4-4 shows that the holes in the waveguide do not affect the waveguiding characteristics of the capillary tubing. The loss in the spectrum is due to the change in the optical path length as the source and detector fibers were being placed before, at, and after the holes. It has been reported in [46] that the presence of perforations do not change the optical transmission of the hollow waveguide.

5.2 Pressure effect and pressure sensing

The results in figure 4-12 and figure 4-13 demonstrate a linear increase in the absorption intensity with applied pressure. Moreover, the data shows that the sensor is capable of gas leak detection at pressures below ambient pressure. Figure 5-3 shows a comparison of the sensor's response as a function of pressure between the 250 mm and 1 mm path lengths sensors. It looks like the 1 mm sensor is less sensitive to pressure change than the 250 mm. This means that the 1 mm sensor can be used in high pressure sensing applications.

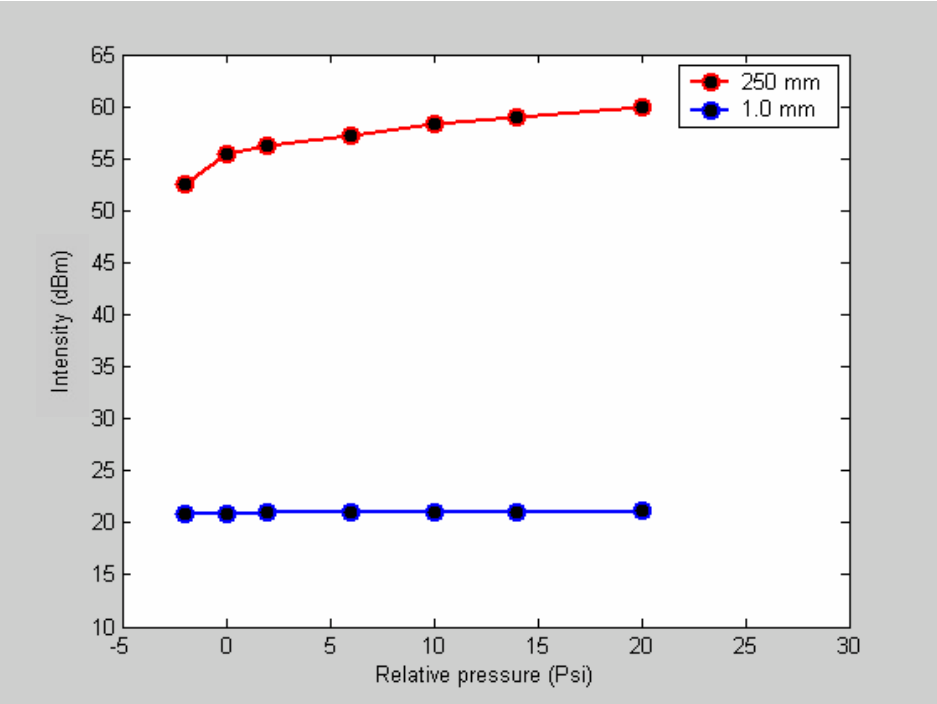

Figure 5-3 Comparison of the sensor's response as a function of pressure

If we ignore all other broadening mechanisms, the absorption lines have natural width. The line width of an absorption line in a spectrum is governed by the Heisenberg uncertainty principle.

$$Linewidth_{natural} = \frac{1}{2\pi c\Delta t} \tag{24}$$

where c is the speed of light and Δt is the lifetime of the excited state. However, natural broadening is not considered in the determination of the width of the lines. Only, Doppler or collision broadening or their combination is considered in line width calculations. The Doppler effect occurs due to the direction of motion of individual molecules with respect to the light passing through it. Doppler broadening varies with temperature and molecular weight but it is independent of pressure. On the other hand, collision broadening is linearly proportional to the pressure. Collision broadening determines the profile of the absorption line when the gas present is at certain pressure level. The half-width pressure broadening is given by

$$Linewidth_{collision} = Linewidth_{atmosphere}\, p \tag{25}$$

where p is the pressure and $Linewidth_{atmosphere}$ is the half-width at 1 atmospheric pressure [50]. The pressure broadening effect observed in figure 4-10 could be valuable since it gives information about the pressure of the detected gas.

5.3 Response time

The response time data can be fitted to the following model.

$$Intensity = a + bt + ce^{-t} \tag{26}$$

where t is time in seconds and a, b, and c are constants. The exponential term represents the fast component and the linear term represents the slower component of the sensor's response. The fit values for the 250 mm sensor are:

$a = 55.97$, $b = -2.80$, and $c = 3.90$ and for the 1 mm sensor the values are: $a = 21.00$, $b = -1.81$, and $c = 0.13$.

Figure 4-12 shows that the intensity drops by 24% after 10 seconds and by 33% after 300 seconds. Whereas figure 4-13 shows that the intensity drops by 46% after 10 seconds and by 75% after 300 seconds. The data clearly shows that the 1 mm sensor has a faster response time than the 250 mm. The reason why it takes a long time to reach 100% intensity drop which corresponds to zero concentration is because of the residual gas in the pipes and hoses of the experimental setup.

5.4 Sensitivity and detection limits.

From the Beer-Lambert law, see section 2.5, one can easily estimate the sensitivity of the sensor. Equation 15 can also be written as

$$I = I_o e^{-\varepsilon c l} \tag{27}$$

For $\varepsilon c l << 1$ equation 27 could be approximated as

$$I \approx I_o (1 - \varepsilon c l) \tag{28}$$

By rearranging equation 28, one could relate the concentration to the change in intensity due to absorption. The minimum detectable concentration could be written as

$$C_{\min} = \frac{\left(\frac{I_o - I}{I_o} \right)_{\min}}{(\varepsilon l)_{\max}} \tag{29}$$

Equation 29 reveals that the detection limit is determined by the path length and the S/N ratio in the spectrum. Since only lines above the noise level in a spectrum can be detected, the reduction of noise can directly correspond to an increase in the detectability. The noise level is a function of the detector, number of scans, spectral resolution and source intensity. The detection limit could be improved by lowering the noise level in the spectrum and increasing the size of the absorption lines. The interrogation system used in this work has an extremely low-noise laser source and can resolve wavelengths down to 0.25 pm. Thus, the system should produce a very low noise level. Additional noise

reduction could be accomplished by using longer measurement time. This was done by setting the system to sweep across the spectrum at a rate of 0.5 instead of default 5 Hz scan rate. Further, lengthening the path length increases the size of the absorption lines. However the limitation on path lengthening is that with a longer light path, the received light intensity would be lower which increases the noise associated with the measurement of the intensity [51]. On the other hand, increasing the source light intensity introduces power saturation. Since absorption of radiation energy from light passing through the sample excites molecules to an upper level, absorption depends on the number of molecules in the lower level. The molecules in the upper level lose energy by collision of molecules with each other and with the walls of the container in order to be in steady-state. Hence, if the input power is too high, molecules will be excited to the upper level at a faster rate then they can fall back to the lower level. This makes the population in the lower level less than that in the absence of light. The fraction of energy absorbed will thus decrease [29].

By using the high-resolution interrogation system a detectable intensity change as small as 0.01 dBm can be measured. The detection limit of the sensor could be calculated from equation 29. For example, having acetylene in a 250mm path length and assuming ε = 0.725 cm^{-1}, the minimum detectable concentration is smaller than 10 ppm. On the other hand, having the same gas in a 1 mm path length results in a minimum detectable concentration of about 1000 ppm. For reference, the standard minimum detection limit as reported in [51] for acetylene in 100 m path length measured in air is 0.15 ppm.

5.5 Sensor miniaturization

Based on the experimental results, the optimal sensor miniaturization will be considered in this section. Sold state chemical sensors such as MOS, ChemFET or CP's offer small dimensionality but have disadvantages such as susceptibility to electromagnetic interference, lack of stability and reproducibility, and some have slow response time. Some of these devices need to be heated to elevated temperatures in order to work. The proposed sensor, which can be miniaturized to the size of the solid state chemical sensors or even smaller, does not only overcome the disadvantages solid state sensors but also offer better performance.

Conventional IR spectroscopy requires optical path lengths greater than 10 cm [49]. The results of sections 4.4 and 4.5 convey that “there's plenty of room at the bottom”, a famous statement by Feynman [52], for further miniaturization of the gas cell in IR spectroscopy. At the same time, the data also shows that there are some limits to how small the sensor can be. These limitations resulted from the design and instruments limitations not theoretical limitation. As we go to smaller dimensions, the response signal also becomes smaller. This means that we have to compete with instrument noise. The experimental results show that the response signal of the 125 μm path length sensor is not observable. This is because the magnitude of the signal is smaller than the noise level. An improved design with better signal processing could relax this limitation.

Moreover, it has been shown both experimentally and theoretically that dielectric hollow waveguides have attenuation that varies with the bore radius. As the bore size gets smaller the signal suffers more attenuation which results in poor detection. The results in chapter 4 show that the intensity of the detected signal increases with increasing the bore size. Larger bore size also results in more interaction between the transmitted light and the gas molecules.

Therefore, for miniaturization design purposes, the gas cell dimensions need to be optimized. Considering the sensor structure and the limitation of the CTS, the optimized dimensional parameters are as follows. A sensor with a gas cell as small as 1 mm long should provide enough optical path length for the transmitted signal. To minimize attenuation and increase the interaction between light and gas molecules a large bore size relative to the wavelength should be used. Based on the proposed design, a sensor with a gas cell volume as small as $5.0\times10^{-13}\,\mathrm{m}^3$ or 0.5 nl (nanoliter) is large enough to produce measurable spectral absorption. This is based on 1 mm path length and bore size of 25 μm. The sensor has already been fabricated and tested as the data suggests in chapter 4.

This miniature gas sensor satisfies all the design requirements and meets the design goals. The decreasing of the sensor’s dimension is advantageous for the following reasons. The sensor does not suffer from bending loss, it is not affected by high pressure changes, and it has a faster response time. However, the small dimensionality affects the sensitivity of the sensor.

Chapter 6: Conclusions and future work

6.1 Conclusions

It has been illustrated in chapter 1 that there is a large variety of chemical sensors. Some sensors can be used in a wide range of applications and some are application specific. A universal senor capable of working in all conditions, which can be also incorporated into any detection/monitoring system, is not possible. It's the task of the designer to select the most appropriate sensor for their application.

Optical sensors offer many advantages over other chemical sensors. They are sensitive, selective, and noninvasive. Additionally, the use of fiber optics technology in optical sensors makes them inexpensive, robust, flexible, miniature, chemically inert, and biocompatible.

The proposed sensor was developed from fiber optics components and technologies. The sensor also operates based on spectroscopic methods and techniques. During the design stage, the sample, sampling method and data quality were considered. To have a better understanding of the sensor's operation and its response, IR sensing and near-IR spectroscopy were reviewed. The derivation of the Beer-Lambert law was presented since it governs the basic principle of the sensor's operations.

The acetylene gas was selected as the gas sample for the sensor testing for two reasons. First the structure of the acetylene molecule makes the gas have strong absorption in the IR region of the electromagnetic spectrum. Second, the acetylene as a gas is an important gas since it is widely used in welding and cutting of metals and in chemical synthesis. The acetylene gas became more important in recent years as its concentration as a pollutant increased in urban and industrial environments. The concern about acetylene increasing concentrations comes from the fact that it is a colorless and extremely flammable gas that targets organs such as the central nervous system and the respiratory system. From the stand point of the study, the acetylene molecule was examined to understand its structure and how it interacts with IR radiation.

In chapter 4, the proposed sensor was tested by direct observation. The gas cell and its waveguiding behavior were investigated. Also, the sensor's response as a function of

different parameters such as the sensor's physical dimensions and applied pressure were examined. Additionally, the sensor's response time was measured as well.

The analysis of the experimental results demonstrated that the proposed sensor meets the design goals by satisfying the requirements identified in chapter 2. The fused silica capillary tubing sensor demonstrated acceptable detection capabilities. The sensor offers benefits such as:

- High sensitivity, selectivity and good detection limit.
- Small dimensionality
- Flexibility
- Immunity to electromagnetic interference
- Wide pressure range operation
- Wide temperature range operation
- Simultaneous gas concentration and pressure measurements.
- Gas leaks detection at pressure levels below ambient pressure
- Fast response time

The miniaturized version of the sensor has advantages and one disadvantage over the large version. The disadvantage is it has a very low sensitivity and the advantages are:

- Very small dimensionality, one millimeter range
- High pressure levels operation
- Very fast response time, less than 1 second.
- Does not suffer from bending loss

In summary, the results of this study point in the direction that the sensor behaves like an IR spectrometer. Thus, a miniature, flexible, inexpensive, chemically inert, biocompatible, sensitive IR spectrometer is being proposed. In addition, this IR spectrometer can be integrated into a large variety of monitoring and detection systems in which it operates under extreme and harsh environments. The sensor could also be used in distributed sensing networks that could provide real time and continuous operation in which it can be remotely accessed, and covers a very large area.

6.2 Future work

In this section, we present some ideas for further improvement of the proposed sensor. There is always a possibility of changing the materials used or the light launching and detection conditions. Moreover, changing the sampling method could also improve the sensing capabilities.

6.2.1 Gas cell material

An alternative to capillary tubing is the use of a hollow waveguide that has its inner wall coated with metal/dielectric reflective coating. This waveguide structure has a metallic layer of silver on the inside of silica glass tubing and then a dielectric layer of silver iodide over the metal film. The waveguide loss can be optimized for the wavelength of interest by controlling the thickness of the dielectric and metallic films [53].

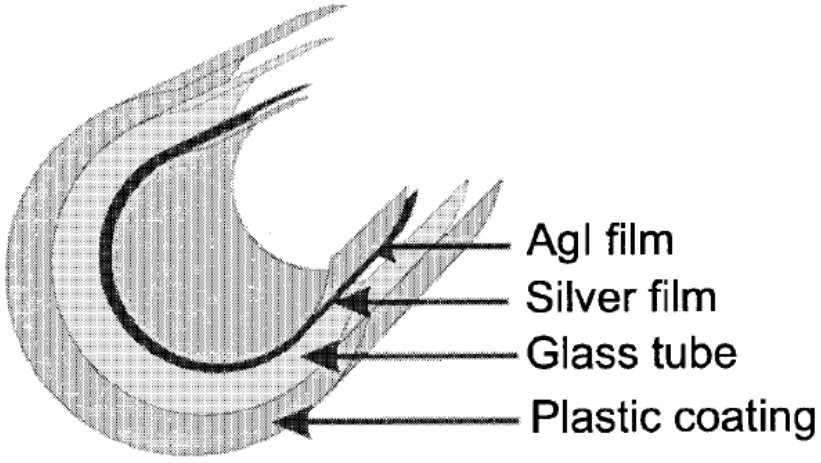

Figure 6-1 Metal/dielectric reflective coating hollow waveguide [53]

Another attractive alternative is the use of hollow core photonic crystal fiber, see figure 6-2. In these kinds of fibers, the hollow core, acting as an extended defect, confines and guides light that have frequency in the bandgap region of the photonic crystal. The fiber can guide light waves efficiently in single mode in which the guiding is independent of the wavelength or hollow core size. Moreover, photonic crystal waveguiding permits a large bend angle which enables the coiling of a long fiber into a small package [54].

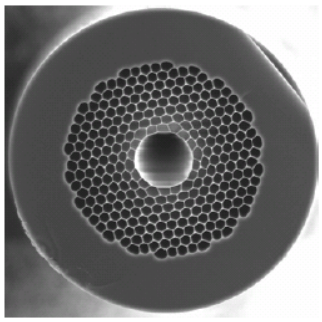

Figure 6-2 Hollow core photonic crystal fiber [55]

6.2.2 Light coupling

The signal transmission through the gas cell could also be improved by improving the coupling of light into the capillary tubing as well as into the receiver fiber. The use of optical components such as lenses and apertures improves the light coupling. For example, launching light with small $f\#$ excites higher-order modes. Thus, optimizing the $f\#$ minimizes the transmission loss [49].

6.2.3 Reflection mode operation

Operating the sensor in reflection mode will decrease the sensor's dimensions significantly. Employing multi-pass techniques for the propagating light, through the gas cell, results in an effective path length longer than the physical path length. This can be done by using highly reflective coating to coat the end surfaces so it will reflect the light back and forth within the gas cell. Even better, photonic crystal reflector is a perfect candidate for this situation since the periodic voids in the structure can serve as gas inlet and outlet.

6.2.4 Signal processing

As we go to smaller dimensions the response signal also become smaller. This means that we have to compete with instrument noise. Using signal processing techniques such as signal amplification and conditioning could improve the response signal of the miniature sensor and also enable further miniaturization.

Moreover, the use of a Fourier-transform infrared (FT-IR) spectrometer improves the S/N per unit time and reduces the spectrum acquisition time to the millisecond timescale. FT-IR spectrum is obtained by first producing interferograms of the light beam that passes through the sample and a reference light beam. Second, these interferograms get transformed into spectra of light with sample absorptions and light without sample absorptions. The ratio of the two spectra gives an FT-IR spectrum [19]. FT-IR instruments that could be coupled to optical fiber are widely available [12].

6.2.5 Sampling method

Instead of relying on diffusion to get the molecules into the path of the optical signal, we can force the gas molecules into the optical path by sucking them into the gas cell. This will speed up the process of getting the molecules in and out of the gas cell. As the molecules flow faster through the gas cell, the sensor's efficiency and sensitivity will increase. To accomplish this one could implement micro electromechanical systems (MEMS) technology in the design of the sensor. Researchers around the world have reported the fabrication of micro size gas pumps and fans by MEMS technology. Figure 6-3 shows an example of a micro fan.

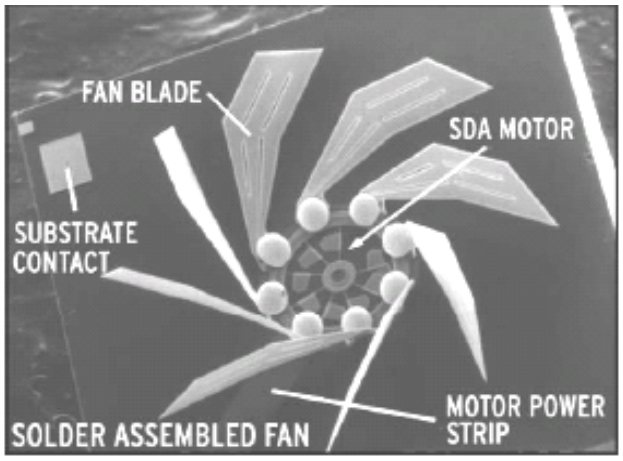

Figure 6-3 Micro Fan [56]

Further improvement in the design could be done by eliminating the fan's motor. This will decrease the space needed for the fan and eliminate the power requirement to power the motor. One way to drive a fan without a motor would be the utilization of the

radiation pressure phenomenon. Based on this phenomenon, it's possible for a laser beam to generate enough torque to rotate a small object. Therefore, it's possible to install a micro fan in the gas cell and drive it by the same laser beam needed for spectral absorption measurements, see figure 6-4.

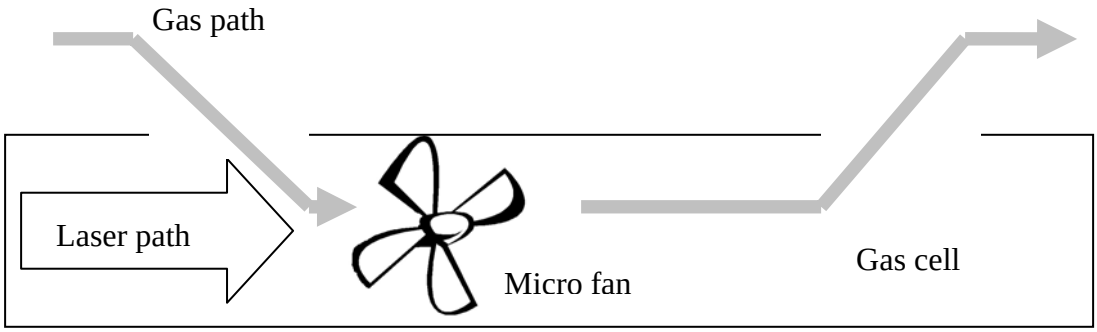

Figure 6-4 Light driven micro fan in gas cell

Light driven rotors have been reported in [57]. The research group has succeeded in building a rotor that changes the direction of rotation by changing the position of the laser focal point relative to the rotor. In figure 6-5, (a) represent the position of the rotor in the focused laser beam, (b) represent the characteristic reflections to drive rotation in one direction, (c) and (d) represent equivalent figures for the rotation in the opposite direction.

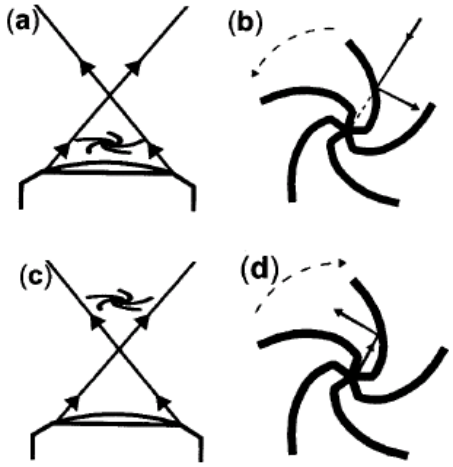

Figure 6-5 Direction of rotation relative to the position of the focused laser [57]

References

[1] S. M. Vaezi-Nejad, "Selected topics in advanced solid state and fiber optic sensors," in *IEE Circuits, Devices and Systems*, vol. 11, R. S. S. D. G. Haigh, J. Wood, Ed. London: The Institution of Electrical Engineers, 2000.

[2] T. C. Pearce, S. S. Schiffman, H. T. Nagle, and J. W. Gardner, "Handbook of Machine Olfaction: Electronic Nose Technology." Weinheim, Germany: Wiley-Vch, 2003.

[3] C. A. Worrell and N. A. Gallen, "Trace-level detection of gases and vapours with mid-infra-red hollow waveguides", *J. Phys. D: Appl. Phys.*, vol. 30, pp. 1984 - 1995, 1997.

[4] L. Hvozdara, N. Pennington, M. Kraft, M. Karlowatz, and B. Mizaikoff, "Quantum cascade laser for mid-infrared spectroscopy", *Vibrational Spectroscopy*, vol. 30, pp. 53 - 58, 2002.

[5] T. A. Blake, J. F. Kelly, T. L. Stewart, J. S. Hartman, S. W. Sharpe, and R. L. Sams, "Absorption spectroscopy in hollow-glass waveguides using infrared diode lasers," in Proc. Diode Lasers and Applications in Atmospheric Sensing 2002, pp. 216 - 232.

[6] C. K. Ho, M. T. Itamura, M. Kelley, and R. C. Hughes, "Review of Chemical Sensors for In-Situ Monitoring of Volatile Contaminants," Sandia National Laboratories, Albuquerque, New Mexico, SANDIA REPORT March 2001 2001.

[7] J. Fraden, *Handbook of Modern Sensors: Physics, Designs, and Applications*, 3rd ed. New York: AIP Press/Springer, 2004.

[8] T. E. Edmonds, "Chemical Sensors." Glasgow: Blackie; Chapman and Hall, 1988.

[9] J. Janata, *Principles of Chemical Sensors*. New York: Plenum Press, 1989.

[10] M. J. Madou and S. R. Morrison, *Chemical Sensing with Solid State Devices*. San Diego: Academic Press, Inc., 1989.

[11] R. F. Taylor and J. S. Schultz, "Handbook of Chemical and Biological Sensors," IOP Publishing Ltd, 1996.

[12] G. Boisde and A. Harmer, *Chemical and Biochemical Sensing With Optical Fibers and Wavequides*. Norwood: Artech House, Inc., 1996.

[13] D. A. Krohn, *Fiber Optics Sensors: Fundamentals and Applications*: Instrument Society of America, 1988.

[14] B. Culshaw and J. Dakin, "Optical Fiber Sensors: Components and Subsystems," vol. 3. Norwood: Artech House, Inc., 1996.

[15] G. Pickrell, W. Peng, and A. Wang, "Random-hole optical fiber evanescent-wave gas sensing", *Optics Letters*, vol. 29, pp. 1476 - 1478, 2004.

[16] W. Peng, G. R. Pickrell, F. Shen, and A. Wang, "Experimental Investigation of Optical Waveguide-Based Multigas Sensing", *IEEE Photonics Technology Letters*, vol. 16, pp. 2317 - 2319, 2004.

[17] J. Workman and A. W. Springsteen, "Applied spectroscopy: a compact reference for practitioners." San Diego: Academic Press, 1998.

[18] G. Stewart, G. Whitenett, P. Shields, J. Marshall, and B. Culshaw, "Design of fibre laser and sensor systems for gas spectroscopy in the near-IR," in Proc. Industrial and Highway Sensors Technology, Bellingham, WA, 2004, pp. 172 - 180.

[19] B. Stuart, B. George, and P. Mclntyre, *Modern Infrared Spectroscopy* John Wiley & Sons, 1996.
[20] D. L. Andrews, "Perspectives in Modern Chemical Spectroscopy," Springer-Verlag, 1990.
[21] J. T. Houghton and S. D. Smith, *Infra-red Physics*: Oxford University Press, 1966.
[22] H. Gunzler and H.-U. Germlich, *IR Spectroscopy: An Introduction* Wiley-VCH, 2002.
[23] G. Gaulitz and T. Vo-Dinh, "Handbook of Spectroscopy," vol. 2: Wiley-Vch, 2003.
[24] A. L. Smith, *Applied Infrared Spectroscopy: Fundamentals, Techniques, and Analytical Problem-solving*, vol. 54: John Wiley & Sons, Inc., 1979.
[25] W. West, "Chemical Applications of Spectroscopy," in *Technique of Organic Chemistry*, vol. 9, A. Weissberger, Ed., 2 ed: Intersciense Publishers, Inc., 1968.
[26] K. E. Stine, *Modern Practices in Infrared Spectroscopy: Laboratory Manual*: Beckman.
[27] K. Kiss-Eross, "Analytical Infrared Spectroscopy," in *Wilson & Wilson's Comprehensive Analytical Chemistry*, vol. VI, G. Svehla, Ed.: Elsevier Scientific Publishing, 1976.
[28] D. N. Kendall, "Applied Infrared Spectroscopy." New York: Reinhold Publishing, 1966.
[29] J. E. Crooks, *The Spectrum in Chemistry*. London: Academic Press Inc., 1978.
[30] N. B. Colthup, L. H. Daly, and S. E. Wiberley, *Introduction to Infrared and Raman Spectroscopy*, Third ed. San Diego: Academic Press, Inc., 1990.
[31] N. L. Alpert, W. E. Keiser, and H. A. Szymanski, *IR: Theory and Practice of Infrared Spectroscopy*, Second ed. New York: Plenum Press, 1970.
[32] F. M. Mirabella, "Modern Techniques in Applied Molecular Spectroscopy," in *Techniques in Analytical Chemistry*: Wiley & Sons, Inc., 1998.
[33] J. H. v. d. Maas, *Basic Infrared Spectroscopy* 2ed: Heyden & Son Ltd., 1972.
[34] *The Book on the Technologies of Polymicro*: Polymicro Technologies, LLC, 2005.
[35] "NIOSH Pocket Guide to Chemical Hazards (NPG)," U.S. Dept of Health and Human Services, Public Health Service, Centers for Disease Control and Prevention, National Institute for Occupational Safety and Health, 2004.
[36] F. Bohlmann, T. Burkhardt, and C. Zdero, *Naturally occurring acetylenes* Academic Press, 1973.
[37] D. Jacquemart, V. D. J.-Y. Mandin, C. Claveau, J. V. Auwera, M. Herman, L. S. Rothman, L. Regalia-Jarlot, and A. Barbe, "The IR acetylene spectrum in HITRAN: update and new results", *Journal of Quantitative Spectroscopy & Radiative Transfer*, vol. 82, pp. 363 - 382, 2003.
[38] T. R. Gilbert, G. Davies, and R. V. Kirss, *Chemistry: Science in Context*: Norton, W. W. & Company, Inc., 2003.
[39] J. W. Hill and R. H. Petrucci, *General Chemistry: An Integrated Approach* 3ed: Prentice Hall, 2001.
[40] R. T. Conley, *Infrared Spectroscopy*. Boston: Allyn and Bacon, Inc., 1966.

[41] S. Sudo, I. Yokohama, H. Yasaka, Y. Sakai, and T. Ikegami, "Optical Fiber with Sharp Optical Absorptions by Vibrational-Rotational Absorption of C2H2 Molecules", *IEEE Photonics Technology Letters*, vol. 2, 1990.
[42] (2005), The HITRAN Database Available: http://cfa-www.harvard.edu/HITRAN/
[43] B. R. Henry, M. A. Mohammadi, and A. W. Tarr, "The overtone spectrum of acetylene: A rotational analysis based on a local model description", *J. Chem. Phys*, vol. 77, pp. 3295 - 3300, 1982.
[44] G. Pickrell, W. Peng, B. Alfeeli, and A. Wang, "Fiber optic chemical sensing," in Proc. Sensors for Harsh Environments II, Boston, MA, USA, 2005, pp. 1-15.
[45] R. C. Denney, *A Dictionary of Spectroscopy*, 2 ed. New York: Wiley & Sons, Inc., 1982.
[46] G. J. Fetzer, A. S. Pittner, W. L. Ryder, and D. A. Brown, "Tunable diode laser absorption spectroscopy in coiled hollow optical waveguides", *Applied Optics*, vol. 41, pp. 3613 - 3621, 2002.
[47] M. Miyagi and S. Nishida, "Transmission Characteristics of Dielectric Tube Leaky Waveguide", *IEEE Transactions on Microwave Theory and Techniques*, vol. MTT-28, pp. 536-541, 1980.
[48] R. H. Micheels, K. Richardson, D. J. Haan, and J. A. Harrington, "FTIR Based Instrument Employing a Coiled Hollow Waveguide Cell for Rapid Field Analysis of Volatile Organic Compounds," in Proc. SPIE Conference on Chemical, Biochemical, and Environmental Fiber Sensors X, Boston, Massachusetts, 1998, pp. 66 - 74.
[49] R. L. Kozodoy, R. H. Micheels, and J. A. Harrington, "Small-Bore Hollow Waveguide Infrared Absorption Cells for Gas Sensing", *Applied Spectroscopy*, vol. 50, pp. 415 - 417, 1996.
[50] J. Wormhoudt, "Infrared Methods for Gaseous Measurements: Theory and Practice," in *Optical Engineering*, vol. 7, B. J. Thompson, Ed.: Marcel Dekker, Inc., 1985.
[51] M. W. Sigrist, "Air Monitoring by Spectroscopic Techniques," in *Chemical Analysis*, vol. 127, J. D. Winefordner, Ed. John Wiley & Sons, Inc., 1994.
[52] R. Feynman, "There's plenty of room at the bottom ", *Journal of microelectromechanical systems* vol. 1, pp. 60-66, 1992.
[53] J. A. Harrington, "A Review of IR Transmitting, HollowWaveguides", *Fiber and Integrated Optics*, vol. 19, pp. 211 - 227, 2000.
[54] P. N. Prasad, *Nanophotonics*: John Wiley & Sons, 2004.
[55] CrystalFiberA/S, (2005), Airguiding Hollow-core Photonic Bandgap Fiber Products Available: http://www.crystal-fibre.com/products/airguide.shtm
[56] R. J. Linderman, P. E. Kladitis, and V. M. Bright, "Development of the micro rotary fan," in Proc. Sensors and Actuators A-Physical, Switzerland, 2002, pp. 135-42.
[57] P. Galajda and P. Ormos, "Rotors produced and driven in laser tweezer with reversed direction of rotation", *Applied Physics Letters*, vol. 80, pp. 4653-4655, 2002.

Vita

Bassam Alfeeli completed two Bachelor of Science degrees both with high honor from the Florida Institute of Technology, Melbourne, Florida. One is in Computer Engineering awarded in May 2000 and the other is in Electrical Engineering awarded in December 2000. In 2001 he joined the Department of Advanced Systems in the Kuwait Institute for Scientific Research, Kuwait as a professional research assistant and then got promoted to professional research associate in 2003. In 2004 he became a graduate student of the Center for Photonics Technology at Virginia Tech. His research interests include the development of sensors related to the oil industry and pollution control. Bassam is also affiliated with the International Society for Optical Engineering (SPIE), the Institute of Electrical and Electronic Engineers (IEEE), and Tau Beta Pi, National Engineering Honor Society.